JCTC Journal of Chemical Theory and Computation

Article

pubs.acs.org/JCTC

Photoisomerization of Stilbene: The Detailed XMCQDPT2 Treatment

I. N. Ioffe*,† and A. A. Granovsky*,‡

†Department of Chemistry, Lomonosov Moscow State University, Moscow, 119991, Russia

‡Firefly Project, Moscow, 117593, Russia

Supporting Information

ABSTRACT: We report the detailed XMCQDPT2/cc-pVTZ study of trans−cis photoisomerization in one of the core systems of both experimental and computational photochemistry—the stilbene molecule. For the first time, the potential energy surface (PES) of the S_1 state has been directly optimized and scanned using a multistate multiconfiguration second-order perturbation theory. We characterize the *trans*-stilbene, pyramidalized (phantom), and DHP-*cis*-stilbene geometric domains of the S_1 state and describe their stationary points including the transition states between them, as well as S_1/S_0 intersections. Also reported are the minima and the activation barriers in the ground state. Our calculations correctly predict the kinetic isotope effect due to H/D exchange at ethylenic hydrogens, the dynamic behavior of excited *cis*-stilbene, and *trans-cis* branching ratio after relaxation to S_0 through a rather unsymmetric conical intersection. In general, the XMCQDPT2 results confirm the qualitative adequacy of the TDDFT (especially SF-TDDFT) picture of the excited stilbene but also reveal quantitative discrepancies that deserve further exploration.

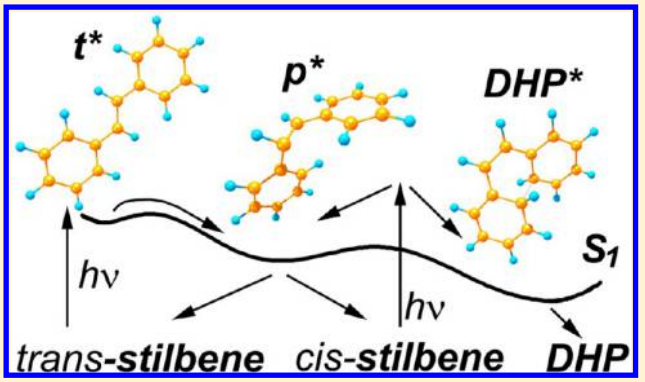

INTRODUCTION

Trans−cis photoisomerization of stilbene is a fundamental example of a broad class of photochemical processes. Twisting around a double bond upon photoactivation can be regarded as a typical motion in molecular machines (see, e.g., ref 1). The stilbene molecule combines a (relatively) simple structure with being a very convenient object for spectroscopic studies. Yet, although stilbene has attracted the interest of photochemists and theorists for decades, there is still no ultimate consensus on the detailed interpretation of its photochemical behavior, and computational investigations of its excited electronic states encounter complications such as reordering and mixing of states at the CASSCF level, as will be discussed below.

A multitude of experimental investigations of stilbene are known to date,[2−81] and their key findings may be summarized as follows. UV excitation of *trans*-stilbene creates an excited electronic state t* with a lifetime which in the gas phase depends on internal vibrational energy, varying from nanoseconds below ∼1700 cm^{-1} to ca. 200 ps at ∼2600 cm^{-1};[2,5,6,9] whereas in low-viscosity solvents it is typically >40 ps.[24,25,31,55] The deactivation is due to crossing of a barrier along a reaction coordinate which is dominated by twisting around the ethylenic double-bond. After the barrier, at about 90° twist angle a so-called "phantom" state p* is reached.[46,55,61] From there, fast internal conversion leads to a mixture of *trans*- and *cis*-stilbene in the electronic ground state with comparable yields.[64] The t* lifetime is characterized by a kinetic isotope effect when the ethylenic hydrogen atoms are exchanged by deuterium; whereas H/D exchange at the phenyl rings shows almost no effect.[6,31] *cis*-Stilbene reaches the phantom state much faster—within 1 ps—and yields a similar mixture of trans- and cis-isomers.[71,73] However about 10% of the excited population rather forms 4a,4b-dihydrophenanthrene (DHP) where the two phenyl rings are linked.[19,64,71,73]

Numerous theoretical studies of stilbene[1,57,82−131] include both quantum chemical studies and modeling of chemical dynamics by means of RRKM theory and its various modifications. However, only few works offer a sufficiently global study of the excited-state potential energy surface (PES). A key post-Hartree−Fock study is due to Quenneville and Martínez[99] who used state-averaged CASPT2//CASSCF(2,2) computations (plus CASSCF(14,12) optimization of conical intersection) to study the path from *trans*- to *cis*-stilbene in the excited state. Their important contribution was the description of a pyramidalized stationary point reached in S_1 upon twisting without symmetry constraints, and of the nearby S_0/S_1 intersection which likely is involved in the photoisomerization. Unfortunately their work was limited to the minimum (2,2) active space and the number of correlated orbitals in the CASPT2 calculations was severely restricted. Recently, Liu and Morokuma,[1] working in the context of exploring larger molecular rotors, reported CASCCF(10,10) PES scans for several exited states, though mostly under the C_2-symmetric constraints. This active space expansion, however, did not add much to the findings of Quenneville and Martínez[99] regarding

Received: July 23, 2013
Published: October 3, 2013

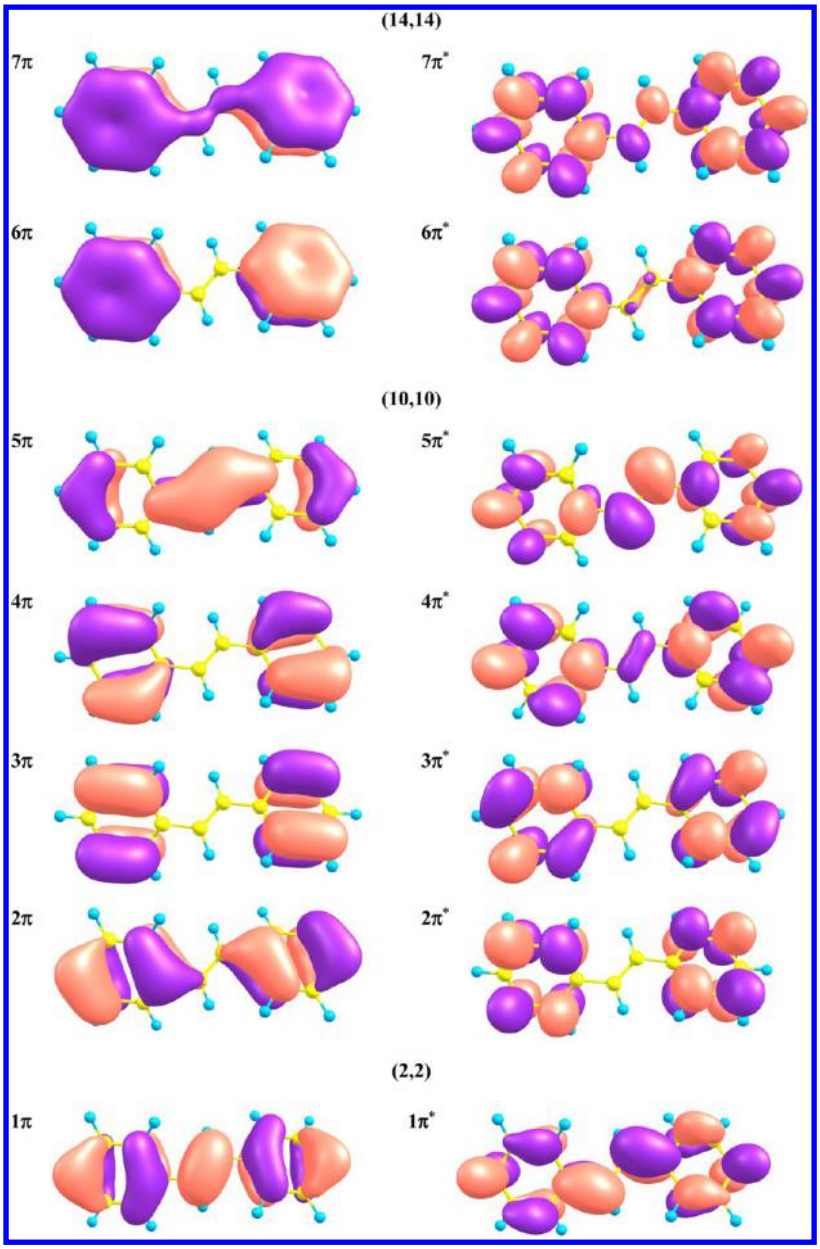

Figure 1. Active spaces used in the present work exemplified by *trans*-stilbene. The (14,14) active space encompasses the complete set of π-orbitals from 7π to $7\pi^*$, the reduced (10,10) space omits 7π, 6π, $6\pi^*$, and $7\pi^*$, and the minimum (2,2) space includes only the HOMO (1π) and the LUMO ($1\pi^*$).

S_1, partly due to indescribability of the pyramidalized geometries under the said constraints and largely due to the fact that pristine stilbene was not central to their work.

Among the DFT-based excited state trackings, an initial attempt by Han, Noodleman, and co-workers[117] used the delta-SCF approach that involved broken-symmetry and spin projection techniques. In the light of more recent works, their results largely lost significance. Later, Improta and Santoro[108] presented TD-PBE0 minimum energy paths (MEPs) and 2D scans of the excited state PES on the trans- and cis-sides, as well as isomerization barriers. The authors predicted, in particular, that unconstrained optimization of excited *cis*-stilbene leads to excited DHP. In 2011, Gordon and Minezawa[129] used the spin-flip TDDFT technique (BHHLYP/DH(d,p)) that partially cures conventional TDDFT for lacking double excitations, to construct a fundamental 2D profile of the whole potential energy surface including the perpendicular region where the two-dimensional (twisting + pyramidalization of one of the central carbon atoms) PES scanning is of particular importance. They described the key stationary points and S_0/S_1 intersections, of which conventional TDDFT is not capable. While the SF-TDDFT results are most insightful (and the conclusions of the present work show many qualitative similarities with their results), high quality ab initio benchmark calculations are still needed as a source of verification and, hopefully, improvement of the TDDFT results.

A common present day standard for high-level calculations of excited states is multistate multireference (MS-MR) perturbation theory in its various implementations. The extended multiconfiguration quasi-degenerate second order perturbation theory XMCQDPT2 has been presented recently[132] as a correction for certain deficiencies of the previously known

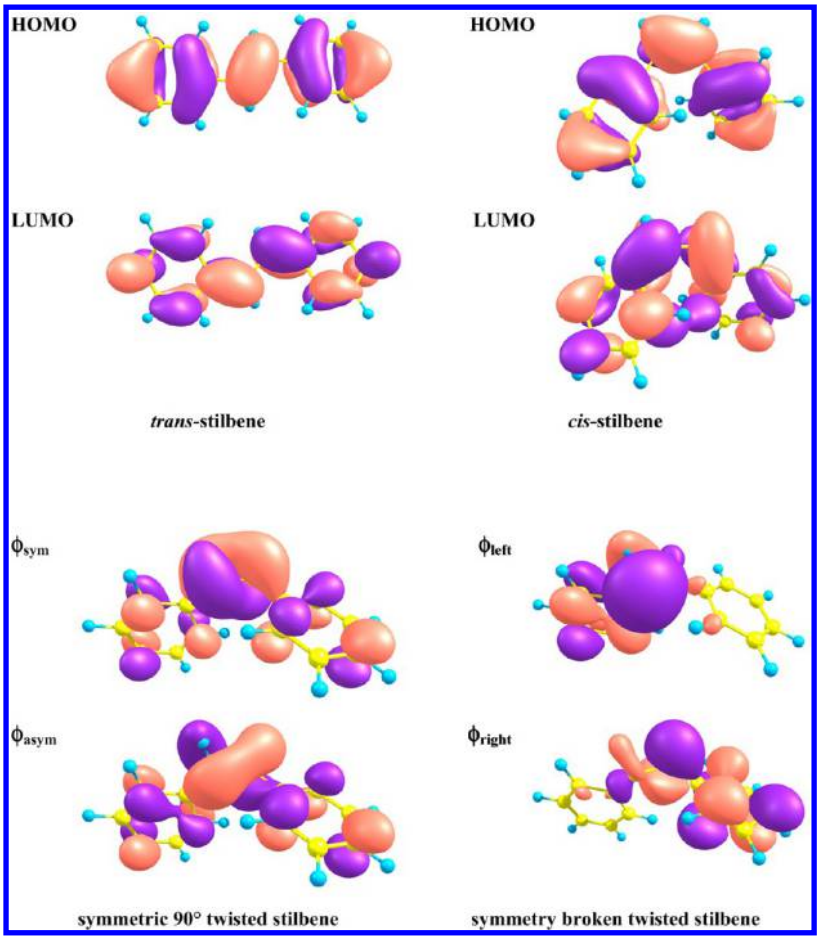

Figure 2. Two boundary orbitals in different geometric configurations of stilbene that are responsible for essential description of the S_0 and S_1 states.

MCQDPT2 approach.[133,134] A similar modification of MS-CASPT2, called XMS-CASPT2, followed shortly.[135] Implementation of XMCQDPT2 in the Firefly quantum chemistry package[136] enables efficient numerical geometry optimizations of ground and excited states directly at the XMCQDPT2 level, both with and without state averaging. This makes it possible to go beyond the commonly used methodology that involves CASSCF geometry optimizations followed by single point (SP) perturbation corrections. In our previous work on transient Raman spectroscopy of excited stilbenes,[57] we already successfully applied XMCQDPT2 optimizations of *trans*- and *cis*-stilbene and even performed vibrational calculations. In the present paper we provide a detailed computational study of the S_1 state of stilbene and of its photochemical aspects.

■ COMPUTATIONAL METHODS

The computations were performed with the Firefly quantum chemistry package version 8.0.0[136] partly based on the GAMESS(US)[137] source code. For scanning the PES, constructing MEPs, and optimizing the key stationary and intersection points, initially we intended to use the CASSCF-(14,14)/cc-pVTZ level of theory with the complete π-orbital active space (see Figure 1), while the proper energy and order of the excited states was to be obtained from single-point XMCQDPT2(14,14) recalculations. However we had to abandon this scheme due to critical shortcomings that arise from the tricky nature of the deceptively "conventional" stilbene molecule.

Even in the nontwisted cis- and trans-regions of its PES, the S_1 state obtained as the second eigenstate of the XMCQDPT2 effective Hamiltonian and observed to be dominated by the single HOMO−LUMO excitation shows highest overlap with only sixth or fifth root of the CASSCF Hamiltonian (or the second or third of the B representation in the calculations with explicit C_2 symmetry) rather than with the lowest excited root, as would be desirable. Thus, CASSCF places the S_1 state unphysically high and gives rise to incorrect couplings with other excited states. As one of the consequences, CASSCF requires state averaging to prevent spreading of the HOMO−LUMO contribution, which dominates the target root according to the XMCQDPT2 results, over the manifold of nearby CASSCF states. While this situation is still tolerable, matters get worse in the transitional twisted and symmetry-broken region. As is well-known (see, e.g., ref 83 for earlier discussions), the *trans*-stilbene HOMO that belongs to symmetric (A) representation of the C_2 group and is bonding for the central ethylenic bond transforms in the course of trans−cis isomerization into the antibonding *cis*-stilbene LUMO. Analogously, the antisymmetric (B) and antibonding *trans*-stilbene LUMO ends up as bonding HOMO of *cis*-stilbene. This results in a quasi-degeneracy of these two orbitals nearly halfway between *trans*- and *cis*-stilbene (about 90° twisting around the central ethylenic bond), their left (ϕ_{left}) and right (ϕ_{right}) halves becoming essentially orthogonal, and consequent quasi-degeneracy of the symmetrized states (see Figure 2)

$$S_1 = 1/\sqrt{2}(\phi_{sym}(1)\phi_{asym}(2) + \phi_{asym}(1)\phi_{sym}(2))$$
$$= 1/\sqrt{2}(\phi_{left}(1)\phi_{left}(2) - \phi_{right}(1)\phi_{right}(2))$$

and

$$S_2 = 1/\sqrt{2}(\phi_{sym}(1)\phi_{sym}(2) + \phi_{asym}(1)\phi_{asym}(2))$$
$$= 1/\sqrt{2}(\phi_{left}(1)\phi_{left}(2) + \phi_{right}(1)\phi_{right}(2))$$

while the ground state becomes essentially a biradical:

$$S_0 = 1/\sqrt{2}(\phi_{sym}(1)\phi_{sym}(2) - \phi_{asym}(1)\phi_{asym}(2))$$
$$= 1/\sqrt{2}(\phi_{left}(1)\phi_{right}(2) + \phi_{right}(1)\phi_{left}(2))$$

Interaction of S_1 and S_2 upon symmetry breaking (for example, pyramidalization of one of the central ethylenic carbons) removes the degeneracy, yielding the new asymmetric excited states that exhibit so-called sudden polarization[138] and may be viewed within the paradigm of the pseudo-Jahn−Teller effect (PJTE).[139]

$$S_{left} = \phi_{left}(1)\phi_{left}(2) \quad \text{and} \quad S_{right} = \phi_{right}(1)\phi_{right}(2)$$

Of these two states, the one localized on the pyramidalized side becomes S_1 while the second one does not necessarily remain S_2 and may even mix with other excitations.

We found that the twisted region of the PES cannot be satisfactorily described at the CAS(14,14) level. In particular, attempts to optimize S_1 as S_{left} ultimately resulted in its irrecoverable mixing with other states in the range between second to sixth CASSCF root. At the same time, S_{right} was obtained as the seventh or even higher CASSCF root, especially when moving from the twisted region toward cis- and trans-configurations. We thus failed to find a CASSCF state-averaging scheme that would yield essentially correct S_1 state as one of the roots and would be, in the same time, uniformly applicable to the whole trans-to-cis path. In view of that, we opted for performing numerical geometry optimizations directly at the XMCQDPT2/cc-pVTZ level of theory where the effective XMCQDPT2 Hamiltonian assembles physically relevant S_1 state from the contributions scattered over various CASSCF roots.

At present, XMCQDPT2(14,14) optimizations are prohibitively demanding, so there was a need to cut the active space. The two obvious choices were (i) to exclude the two lowest and two highest lying π-orbitals localized on phenyl moieties and utilize the remaining (10,10) space or (ii) to perform a more radical truncation to the minimum (2,2) space (see Figure 1). Although the minimum space may not describe static correlation accurately, it has an important advantage over the larger active spaces, one that is associated with the problem of intruder states. In larger calculations such states emerge inevitably and must be countered by "intruder state avoidance" (ISA) shifts of the energy denominators or similar techniques. Small active spaces quite often do not require this artificial correction.

In view of the above considerations, we selected the following strategy. The PES of the S_1 state was studied at the XMCQDPT2/SA3-CASSCF(2,2)/cc-pVTZ level of theory (i.e., by optimizing the second XMCQDPT2 root within the (2,2) active space using a state-averaged semicanonical Fock operator) without symmetry restrictions. State averaging over all three singlet states was intended to provide a balanced description of the whole PES with its symmetry broken regions where interactions with other states from the minimum active space became significant (hereinafter we will use brief designations like SAx-XMCQDPT2(m,n) where the same equal-weight averaging is implied for the CASSCF stage and in constructing the zero order Hamiltonian of XMCQDPT2). An additional benefit of such treatment is its exact size consistency. We also used XMCQDPT2(2,2) geometry optimization without state averaging for C_2-symmetric excited *trans*-stilbene where interaction of S_1 with the other states of the minimum space vanishes by symmetry. Ultimately, we employed the most elaborate XMCQDPT2(10,10) geometry optimizations with various state-averaging schemes, 12 states in the XMCQDPT2 model space, and with or without the use of symmetry to (i) optimize the key energy minima in S_1 and (ii) to track the states located close to S_1 and not describable with the minimum active space. With the (10,10) active space, our tactics was to use uniformly broader state-averaging to compare energy at varying geometries but as narrow averaging as possible in case of geometry optimizations.

Careful selection of both the state-averaging scheme and the size of the model space is of critical importance to reliably set up a QDPT calculation. One can typically expect two effects of the opposite sign. The extension of a model space by incorporating some higher-energy roots into it generally improves the description of the target, lower energy states of interest.[132] This can be explained by the analogy with the variants of a perturbation theory based on the intermediate Hamiltonian techniques.[140] In addition, incorporation of higher-energy roots effectively partially decontracts reference CASCI vectors thus allowing more flexibility in the description of target states. In our case, selection of the twelve-state model space was based on experimentation with quantitative stability of the results for S_1.

On the contrary, broader state averaging in the SA-CASSCF procedure typically worsens the description of each individual state entering state-averaging. However, stilbene is a striking example of a system where without state-averaging one cannot correctly recover the electronic state of interest. As the good description of zero-order states is very important to any perturbation theory based approach, one needs to find a good compromise.

In view of that, for the geometry optimizations only those CASSCF roots were included in averaging that gave important contributions to the zero-order part of the QDPT wave function of S_1 (generally above 0.03 by weight) and also, inevitably, the ground state root for the geometries close to state crossings. By doing so we intended to prevent overestimation of the dynamic correlation effects expectable in case of compromised CASSCF description of the state of interest in the framework of broader state averaging. However, to compare energy at different geometries in a balanced way, one would rather prefer broader averaging (in the present case, six CASSCF roots or five whenever inclusion of the ground state was unnecessary) in order to properly recover all major contributions to S_1 while keeping the set of equivalent CASSCF root sufficiently homogeneous over the whole PES.

The adequacy of XMCQDPT2 optimizations with (2,2) and (10,10) was confirmed on a set of important geometric configurations by reference SA6-XMCQDPT2(14,14) single point calculations with 12 states in the XMCQDPT2 model space, also without explicit use of symmetry. In this case, averaging over the six lowest states in the CASSCF procedure

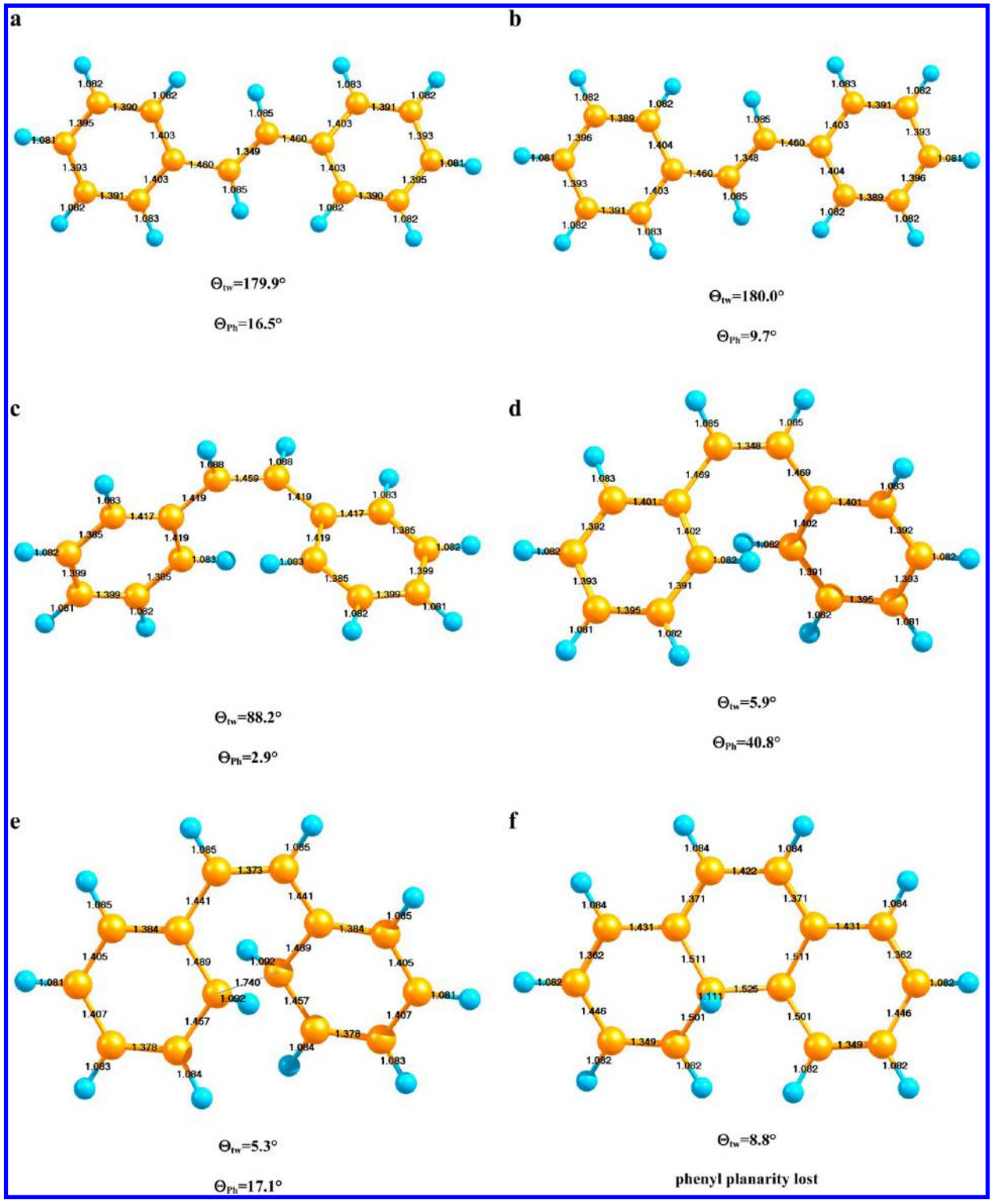

Figure 3. Optimized ground state geometry of (a) C_2 *trans*-stilbene, MP2; (b) C_i *trans*-stilbene, MP2; (c) C_2 trans-to-cis transition state, SA3-XMCQDPT2(2,2); (d) C_2 *cis*-stilbene, MP2; (e) C_2 cis-to-DHP transition state, SA3-XMCQDPT2(2,2); (f) C_2 DHP, MP2. Dihedral twisting angles at the central ethylenic bond (Θ_{tw}) and phenyl rotation angles with respect to the central bond (Θ_{Ph}) are indicated.

ensures proper inclusion of S_1 in the CASSCF solution at all geometries of interest within an adequately uniform set of averaged states, including the ground state for better description of the respective excitation energies. Although some of the said six states do not contribute to S_0 and S_1, we found the SA6 scheme to be the most appropriate for description of *trans*-stilbene. Indeed, we found that the second and the third CASSCF roots of the *B* representation must be included to properly encompass the HOMO−LUMO excitation, the first *B* root mixes with them at the XMCQDPT2 level, and inclusion of the two excited state *A* roots is required to prevent mixing with the *B* roots and ensuing symmetry breaking, which we observed at *trans*-stilbenic geometries, yet another manifestation of the PJTE.[139]

dx.doi.org/10.1021/ct400647w | J. Chem. Theory Comput. 2013, 9, 4973−4990

All calculations were performed with frozen chemical core (and no other restrictions on the correlated orbitals) and, except for the (2,2) active space, with an ISA shift of 0.02 hartree. All geometry optimizations were carried out using high precision numerical gradients, and vibrational calculations were based on numerical differentiation of the latter. No symmetry restrictions were applied unless the presence of symmetry (generally C_2) became apparent from high precision symmetry-less optimization. Optimization of intersections of the electronic states were carried out using either the penalty function approach or the Lagrange multiplier-based sequential quadratic program (SQP) optimization to a gap of ~3 meV.

The effects of the intruder states are unphysical diagonal elements and large off-diagonal couplings in the effective XMCQDPT2 Hamiltonian. Such elements are very sensitive to geometric distortions that decouple the XMCQDPT2 states from the intruder ones. Therefore the presence of the intruder states becomes instantly revealed by unphysically large numerical gradients of the energy. As we observed for the minimum (2,2) space, this problem became appreciable only near the ground state geometries of stilbene while no relaxed PES scans constructed for the S_1 state were affected. This made possible, as was intended, to use no ISA shift in the calculations with the (2,2) active space.

To complement the above methodology used for the excited states, the ground state optimizations were carried out at the MP2/cc-pVTZ level of theory with frozen chemical core. For *trans*-stilbene, we also performed frozen core numerical MP4(SDQ)/cc-pVTZ optimization.

Molecular structure visualization presented herein is performed with the aid of the Chemcraft software.[141]

Ground State, Vertical Excitation Energies, and the Lowest Excited States. The MP2/cc-pVTZ ground state geometry of *trans*- and *cis*-stilbene has been already described in our earlier paper.[57] Briefly, *trans*-stilbene is calculated as C_2- and C_i-symmetric stationary points without appreciable twisting around the central ethylenic bond, but with phenyl rings rotated out of plane by 16° and 10°, respectively. The energy difference is only ca. 2 meV in favor of the C_2 conformation. We further optimized the C_2 conformation at the MP4(SDQ)/cc-pVTZ level and observed totally negligible deviations from the MP2 results. Note that these predictions are corroborated by the recent liquid crystal NMR study supported by MP2/6-31G* calculations.[142] Earlier experimental suggestions of nonplanarity of *trans*-stilbene also come from gas phase UV photoelectron spectroscopy[143] and gas phase electron diffraction[144] at elevated temperatures, as well as from X-ray diffraction study at 77 K,[145] though in the latter work the average phenyl torsion in the crystalline phase was found to be below 10°. On the contrary, high resolution spectroscopic studies in jet cooled molecular beams led to conclusions on planarity of *trans*-stilbene (C_{2h}) in both S_0 and S_1.[41,43,74] MP2/6-31G* analysis of vibrational corrections suggests vibrational quasi-planarity as a reconciliatory explanation.[101]

In general, there is no theoretical consensus on the planarity of *trans*-stilbene, various correlated ab initio and DFT calculations providing different predictions (see, e.g., ref 105 where, however, the authors still conclude planarity). In any case, since the respective energy differences have an order of some 10 meV at most, it is unquestionable that the ground state PES near the stationary point is quite flat along the phenyl rotation coordinates. We found the planar C_{2h} geometry, whose energy estimates the barrier between the stationary points from above, to lie only 5 meV above the C_2 conformation.

The ground state of *cis*-stilbene and DHP, as well as the SA3-XMCQDPT2(2,2)-optimized trans-to-cis and cis-to-DHP transition states in S_0, also exhibit C_2 symmetry. The geometry of all these states is shown in Figure 3.

At the MP2/cc-pVTZ level, *trans*-stilbene is 87 meV (92 meV with the zero point energy correction, 87 meV for $\Delta H(298)$) more stable than the *cis*-isomer. This value is remarkably close to the experimental gas-phase calorimetry-based data and the G3MP2 calculation (89 ± 44 and 76 meV, respectively).[146] The equilibrium studies in benzene provide a higher value of 185 meV,[147] which is in better agreement with various B3LYP estimates,[104,118,119] but the liquid phase experimental data[146] suggest possible condensed phase effects. SP-SA6-XMCQDPT2(14,14) data provide comparable 104 meV and barrier height of 2.0 eV for trans-to-cis isomerization in S_0. The ISA-free SA3-XMCQDPT2(2,2) calculations cannot be used directly for determining the barrier since they suffer from intruder states near the trans and cis stationary points. However, a good agreement between the data obtained with different active spaces can still be demonstrated: a combination of $E(trans\text{-}S_1)-E(trans\text{-}S_0)$ from sp-SA6-XMCQDPT2(14,14) and $E(S_0^{\neq})-E(trans\text{-}S_1)$ from SA3-XMCQDPT2(2,2) provides the same barrier height within 20 meV. Another important ground state stationary point, the one of DHP, is found 1.81 eV above *trans*-stilbene at the MP2 level or 1.76 eV after SA6-XMCQDPT2(14,14) recalculation. The DHP-to-cis activation barrier of only 0.72 eV (SA6-XMCQDPT2(14,14), transition state optimized at the SA3-XMCQDPT2(2,2) level) evidences very limited stability of DHP. Unfortunately, very few computational ground state barrier estimates exist in the literature: a somewhat lower DFT value of 1.8 eV was obtained for trans-to-cis isomerization,[117] and strongly underestimated cis-to-trans and cis-to-DHP barriers (below 1 eV) were found with IVO-MRMP calculations.[131]

The vertical SA6-XMCQDPT2(14,14) excitation spectrum of *trans*- and *cis*-stilbene is given in Table 1. In both cases S_1-S_3 form a quasi-degenerate manifold while S_4 lies appreciably higher. We found no intense optical transitions to those states above S_3 that fall into a common UV−vis spectral window. Earlier it was shown that for *trans*-stilbene MS-CASPT2(14,14) predicts an even distribution of the HOMO−LUMO excitation over the two lowest B states separated by 0.3 eV.[97] On the other hand NEVPT2(14,14), in both state specific and quasi-degenerate versions and partially and strongly contracted

Table 1. Vertical Excitation Spectra of *trans*- and *cis*-Stilbene (SP-SA6-XMCQDPT2(14,14))

state/ symmetry (C_2)	excitation energy eV	osc strength	contribution of the HOMO−LUMO excitation (approx)
trans-stilbene			
$S_1(B)$	4.17	0.71	63%
$S_2(A)$	4.31	0.00	
$S_3(B)$	4.35	0.17	14%
$S_4(A)$	5.10	0.00	
cis-stilbene			
$S_1(B)$	4.35	0.04	15%
$S_2(B)$	4.43	0.30	62%
$S_3(A)$	4.56	0.00	
$S_4(A)$	5.50	0.08	

variants, yields S_1 as an essentially pure HOMO−LUMO state and finds a much larger gap of >0.7 eV to the next *B* state.[109] Also to be mentioned is the recent IVO-CASCI(14,14) and IVO-MRMP(14,14) study[131] based on a CASCI reference with nonvariational orbitals: it predicts the separation of the two states closer to that of NEVPT2 but finds a low weight of the HOMO−LUMO excitation (<0.5) in S_1 at the MRMP level. As follows from Table 1, our XMCQDPT2 results regarding HOMO−LUMO contributions fall in between the NEVPT2 and CASPT2 predictions, despite the fact that the calculated gap is even lower than that given by MS-CASPT2. We also confirm that it is the HOMO−LUMO excitation that must be responsible for the observed oscillator strengths. The XMCQDPT2 vertical excitation energy of 4.17 eV exceeds the NEVPT2 and MS-CASPT2 values by 0.2−0.35 eV. Direct comparison of these values with the experimental data is, perhaps, not very meaningful since *trans*-stilbene demonstrates rather broad absorption band with partially resolved vibrational progression (see, e.g., ref 67). However, there is a surprisingly good agreement of our estimate with the band maximum of ca. 4.2 eV reported in hexane.[148] One has to note, however, that the solution phase spectra tend to demonstrate solvent dependent shift to the red.[26]

Optimization of *trans*-S_1, as described in the next section, modifies the structure of the excited states: the S_1-S_2 gap increases to above 0.4 eV while the HOMO−LUMO excitation and the respective oscillator strength concentrate in S_1. This makes S_1 adequately describable by means of the minimum active space as will be further shown below. The respective 0−0 transition energy was calculated as 3.72−3.82 eV (sp-SA6-XMCQDPT2(14,14)) depending on whether XMCQDPT2-(2,2) or (10,10) was used to optimize S_1 and with what state averaging; or further 0.1 eV lower if zero point vibrational corrections are applied (MP2/cc-pVTZ for the ground state and SA3-XMCQDPT2(2,2) for the excited state). High resolution spectroscopic studies[2,4,43,74] report somewhat higher 0−0 transition energy of 4.0 eV on the basis of the vibrationally and rotationally resolved gas phase fluorescence excitation spectra, the value which was reproduced very closely by SF-TDDFT with the BHHLYP functional[129] and some functionals within the conventional LR-TDDFT approach.[109] While XMCQDPT2 somewhat underestimates the energy of the 0−0 transition, possibly as a result of too broad state averaging, it seems to perform better than both partially and strongly contracted QD-NEVPT2(14,14)[109] and MS-CASPT2-(14,14),[97] which gave the vertical excitation energy within the range of 3.8−4.0 eV. Indeed, since correction for relaxation in S_1 is mainly associated with stretching coordinates rather than with any nonplanarities and, therefore, it should be of comparable magnitude in all second-order perturbation theories (PT2), one may expect the adiabatic CASPT2 and NEVPT2 estimates to be not higher than 3.6 eV.

In *cis*-stilbene, similarly to the *trans*-isomer, of the three closely spaced lowest excited states two are of *B* symmetry and comprise unequal contributions of the HOMO−LUMO excitation. However it is now S_2 rather than S_1 that will be populated with higher abundance upon optical excitation of S_0, even though the S_1-S_2 gap is negligible. As will be shown below, relaxation of the vertically excited *cis*-stilbene results in considerable geometric distortion, which leaves little sense in estimating the parameters of the 0−0 transition. With regard to the excitation energies, we observe considerable difference from the earlier PT2 data. The CASPT2(14,12) calculations predicted the HOMO−LUMO state to be S_3 with much larger separation from S_1 (0.5 eV) and S_2; however they employed a less flexible basis set and a smaller active space.[96] The IVO-MRMP(14,14) calculation places, on the contrary, the HOMO−LUMO state below and reports even higher gap of 0.65 eV to the second *B* state.[131] The experimental maximum of the broad structureless absorption band of *cis*-stilbene in hexane is observed at ca. 4.5 eV.[148] Both our XMCQDPT2 value of 4.43 eV and the CASPT2 one of 4.61 eV demonstrate good agreement with the experimental value while IVO-MRMP gives considerable underestimation (4.04 eV).

In view of low separation between S_1-S_3, the applicability of the minimum (2,2) active space to the description of relevant stationary points and MEPs in S_1 requires additional justification. Therefore we undertook optimization of S_1-S_3 in both trans- and cis-configurations at the SA5-XMCQDPT2-(10,10) level with averaging over the five lowest excited states (the inclusion of the ground state was unnecessary since it demonstrated no appreciable interaction with any excited states at those geometries where state reordering was potentially expectable). Interestingly, upon the reduction of the active space from (14,14) to (10,10) we observed an increase of the gap between the S_1, which becomes a clear HOMO−LUMO dominated state in both trans- and cis-isomers (i.e., reordering of S_1 and S_2 occurs in the latter), and the other excited states by ca. 0.5 eV, even though the orbitals omitted from the (14,14) space had occupation above 1.93 or below 0.05 in all states from the S_1-S_3 manifold. This observation demonstrates that the issue of properly selecting the active space is vital for the accuracy of the relative energy of states. Interestingly, the QD-NEVPT2 results[109] do not show a comparably pronounced effect; they predict a considerable separation of states with any of the active spaces used.

The *trans*-S_3 (B) state was found to be unstable with respect to symmetry breaking and ultimately relaxed into the *trans*-S_2 (A) The latter state was found to have a C_{2h}-symmetric stationary point 0.3 eV above S_1 (SP-SA6-XMCQDPT2-(14,14)). We conclude that the higher excited states on the *trans*-stilbene side are unlikely to play important role in the evolution of the photoexcited molecule. For *cis*-stilbene, however, tracking of the accompanying states turned out to be more problematic. The easiest case was *cis*-S_3 (*A*): we observe barrierless twisting toward the perpendicular geometric configurations where this state ultimately becomes S_2 and interacts with S_1 with symmetry breaking as described in Computational Methods. On the contrary, the behavior of the non-HOMO−LUMO *B* state obtained as *cis*-S_2 in SA5-XMCQDPT2(10,10) and *cis*-S_1 in SA6-XMCQDPT2(14,14) remains not fully rationalized. It turned out that XMCQDPT2-(10,10) optimization of this state was repeatedly and reproducibly coming to an unexpected bifurcation in the underlying CASSCF wave function, irrespective of the state-averaging scheme employed. Most surprisingly, such behavior was observed even in calculations based on the nonaveraged ground state CASSCF solution, both with and without explicit use of symmetry. Although indications of symmetry breaking in *cis*-S_2 were observed, we were unable to confidently confirm symmetry breaking interaction with *cis*-S_3 (A) analogous to that observed in *trans*-stilbene.

Nevertheless, since no low lying stationary points were observed in *cis*-S_2 while relaxation of *cis*-S_1 was accompanied by a considerable drop in energy as described in detail below, we may discard all the interfering excited states and concentrate on

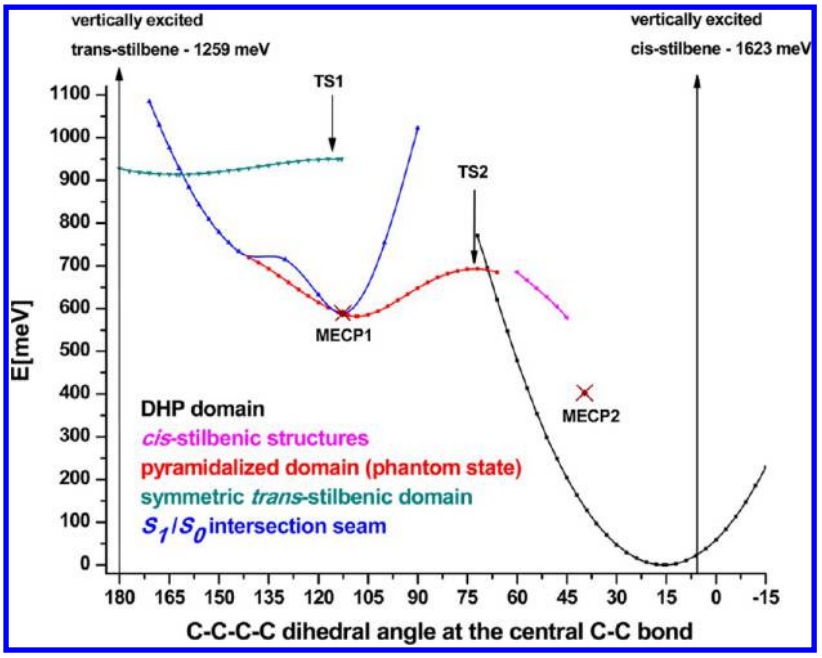

Figure 4. Relaxed scans of the PES of S_1: various domains and characteristic points, locally or globally stable, upon constraining the photoisomerization twisting coordinate (SA3-XMCQDPT2(2,2) results; see also Table 2). TS1—transition state between *trans*-stilbene and the pyramidalized (phantom) state; TS2—transition state between the pyramidalized state and the DHP domain; MECP1—S_1/S_0 minimum energy crossing point in the pyramidalized domain; MECP2—same in the DHP domain (see details in further sections).

Table 2. Relative Energy (meV) of Some Key Points of the PES of S_1

	SA3-XMCQDPT2(2,2) ISA = 0.0	SA3-XMCQDPT2(2,2) ISA = 0.02	SA6-XMCQDPT2(10,10) ISA = 0.02	SP-SA6-XMCQDPT2(14,14)[a] ISA = 0.02
stationary point, *trans*-stilbene	913	884	663	530
trans-to-pyramidalized transition state (**TS1**)	950	*b*		583
stationary point, pyrmidalized state	581	548	~470[c]	319
pyramidalized-to-DHP transition state (**TS2**)	693			485
stationary point, DHP	0	0	0	0

[a]Single-point recalculation at the geometries of column 1. [b]Optimization of the transition states was not performed. [c]Lower tolerance of energy convergence due to S_1/S_0 crossing for the selected averaging.

the HOMO−LUMO dominated S_1. It can be firmly stated that, apart from some interaction near the ground state geometries, S_1 showed no tendency to interact with any electronic state from outside of the minimum active space. Our approach is further justified by the most recent time-resolved fluorescence study[53] where a conclusion has been made that the evolution of the excited *cis*-stilbene occurs within a single one-photon allowed state.

Principal Domains of the PES of S_1 and Justification of the Minimum Active Space. In Figure 4, we present SA3-XMCQDPT2(2,2) relaxed scans of the PES of S_1 along the principal photoisomerization coordinate—the C−C−C−C dihedral angle of twisting around the central ethylenic bond. It was found that the potential energy surface can be subdivided into several domains. In the present section we will provide their general description, to be followed with detailed discussions separately. Upon excitation of S_1 in the *trans*-stilbene, it relaxes into a rather flat C_2-symmetric domain with a stationary point near 170°. Upon twisting, excited *trans*-stilbene passes the transition state TS1 and shortly afterward (near ca. 113°) develops symmetry breaking, which includes considerable pyramidalization of one of the central ethylenic carbon atoms. The excited molecule thus relaxes into the domain of the pyramidalized (or phantom) state. By scanning the twisting angle in this pyramidalized domain back toward 180°, one ultimately arrives (beyond 141°) at the seam of the S_0/S_1 intersection, which also exhibits considerable pyramidalization and the lack of symmetry. The seam remains a locally stable minimum energy path (MEP) in S_1 up to energies well above those of the symmetric *trans*-stilbene. In the range below 141° where the constrained minima depart from the intersection seam, these two relaxed scans remain more or less close to each other down to ca. 110° and then show pronounced divergence.

Moving from the perpendicular state toward *cis*-stilbene, the excited molecule gradually loses pyramidalization and shows a general trend toward regaining C_2 symmetry. Then, however, it passes a barrier and ultimately drops into the DHP domain, the lowest of three major domains in S_1. This domain is characterized in that the phenyl rings come closer to each other and their respective atoms show prebonding trends with partial pyramidalization toward each other, as it will be shown below. Scanning the twisting coordinate from DHP back toward the pyramidalized domain shows divergence of forward and backward PES scans only in a narrow range of twisting angles with their subsequent merger.

We also observed a narrow range of twisting angles where the true *cis*-stilbenic structures, i.e. C_2-symmetric and not showing the tendency of linkage between phenyl rings, were obtained as local constrained minima in S_1. However, these structures are stable only locally and subject to the twisting angle constraint. They do not form unconstrained local minima, neither at the SA3-XMCQDPT2(2,2) level nor in XMCQDPT2(10,10) optimizations with various state averaging schemes. As we will show below, more appropriate description of the said *cis*-stilbenic structures can be provided with the use of a different type of constraint.

To investigate the adequacy of the minimum active space, we also performed optimization of the local minima in S_1 at the same SA3-XMCQDPT2(2,2) level with ISA = 0.02 and at the SA2-XMCQDPT2(10,10) level (ISA = 0.02; averaging over the two lowest B states for the trans-domain and over S_0 and S_1 in the other two domains; we did not optimize transition states at these levels since reliable convergence of their geometries proved to be an exceedingly time-consuming task) and, most importantly, single point recalculations of the five stationary points (local minima + transition states) at the SA6-XMCQDPT2(14,14) level. The results thus obtained are given in Table 2. As one can see, the complete π-orbital active space predicts lower drops in energy when going from *trans*-stilbene to DHP. However, the qualitative picture seems to remain the same. The SA6-XMCQDPT2(10,10) optimization of the three energy minima results in relative energy values rather close to the SP-SA6-XMCQDPT2(14,14) results. Indeed, the orbitals covered by the expansion of the active space from (2,2) to (10,10) provide more important contributions to the lower excited states than the ones completing the (10,10) space to (14,14). It is to be noted, however, that at all geometries considered, we found that all orbitals outside the (2,2) active space have occupancies either above 1.90 or below 0.10. This may serve additional empirical justification of applicability of the minimum active space.

Regarding the quantitative accuracy, it is not very straightforward to judge what results of Table 2 are more correct. As one can see, the effect of the ISA shift on the minimum active space is rather limited, though noticeable. Therefore, comparably limited must be its effect on the same dominating configurations when considered within the broader active spaces. State averaging, however, is a factor which is more difficult to rationalize. To add to the data given in Table 2, we performed SA2-XMCQDPT2(10,10) calculations; the principal contributions to S_1 were covered by averaging over the CASSCF S_0 and S_1 roots for the DHP and the pyramidalized stationary points, and over the two lowest roots of the B representation for the C_2-symmetric *trans*-stilbenic configuration. These SA2 results were incorrect even qualitatively as they placed the pyramidalized state ca. 0.12 eV above the excited *trans*-stilbene, contrary to the very fact of *trans*-stilbene isomerization. However, comparing alone the cases of averaging over closely located S_0 and S_1, namely the pyramidalized minimum and the DHP one, the SA2-XMCQDPT2(10,10) energy difference was 589 meV, remarkably close to the SA3-XMCQDPT2(2,2) results. These observations point at the issues of stability of the XMCQDPT2 (and generally MS-MR-PT2) results is the situation when various state-averaging schemes are required for correct descriptions of the states of interest. For this reason, we were bound to use broader state averaging uniformly applicable to all geometries and electronic states being compared despite possible worsening of the CASSCF description of the target states and, consequently, possible overestimation of the dynamic correlation computed by means of perturbation theory. Possibly, some improvement may be achieved in future through assessment of the alternative variants of the zero order XMCQDPT2 Hamiltonian, as was briefly discussed in ref 149.

Comparing our findings to the literature data, we see that the CASSCF(2,2) picture of S_1 state correctly predicts the asymmetric pyramidalized minimum in S_1.[99] However, its depth with respect to (wrt) the *trans*-stilbenic stationary point (>0.5 eV) seems overestimated. More importantly, it predicts a *cis*-stilbenic stationary point instead of a DHP-like one, which is in qualitative disagreement with the present work as well as with TDDFT treatment.[108,129] In the CASSCF(10,10) study of ref 1, unfortunately under C_2 symmetry constraints, optimization of the excited *cis*-stilbene did not lead to DHP-like geometries as well; according to their Figure 3, they have rather located some shallow energy minima in S_1 at the twisting angles of ca. 60 and 120°. Finally, in our CASSCF(14,14) optimization, we also observed a *cis*-stilbenic local minimum in S_1 that was perfectly stable with respect to deformation toward DHP. These computational results corroborate the conclusion of Minezawa and Gordon that proper reproduction of the DHP-like stationary point depends on the inclusion of dynamic correlation rather than on the size of the active space.[129] It also has to be noted that CASSCF(14,14) with symmetry constraints does not confirm the details of the ^1B PES of Figure 3 of ref 1 but reveals only the planar *trans*-stilbenic stationary point and the lower *cis*-stilbenic one with twisting angle of ca. 30°.

Turning to the known TDDFT results,[108,129] we note good qualitative agreement. Especially valuable is the SF-TDDFT treatment,[129] which makes accessible the pyramidalized domain of the PES of S_1. Unfortunately, the computational demands of our XMCQDPT2 methodology prevent us from reproducing their two-dimensional (twisting-pyramidalization) scan. There are, however, significant quantitative discrepancies. Most importantly SF-TDDFT predicts virtually isoenergetic trans and pyramidalized stationary points in S_1. If true, this would result in an equilibrium between these two configurations, which is not observed in the experiment. Furthermore, the S_0/S_1 crossing point is predicted to lie somewhat too high with respect to the pyramidalized minimum, taking into account the very low experimental lifetime of the phantom state.[55] In better agreement with our results is the SF-TDDFT energy difference between the trans and DHP stationary points (~0.4 eV); still it is below our SP-SA6-XMCQDPT2(14,14) estimate.

Excited *trans*-Stilbene, Initial Stage of Trans-to-Cis Isomerization, and the Kinetic Isotope Effect. The trans-domain of the PES of the S_1 state is the only one that reproducibly retains the C_2 symmetry at various levels of theory. While the PES of S_1 is flattest in the *trans*-stilbene domain, the lifetime of the excited *trans*-stilbene is larger than that of the phantom and *cis*-stilbenic states, which can be associated with a low extent of initial vibrational excitation of the twisting coordinate due to almost planar central C—C═C—C unit in the ground state. Computationally, the C_2 symmetric excited molecule allows for pure state XMCQDPT2-(2,2), i.e. MRMP2 treatment of S_1 since it is the only state of B symmetry within the minimum active space, as well as allows for averaging only over the B-symmetric states at the XMCQDPT2(10,10) level.

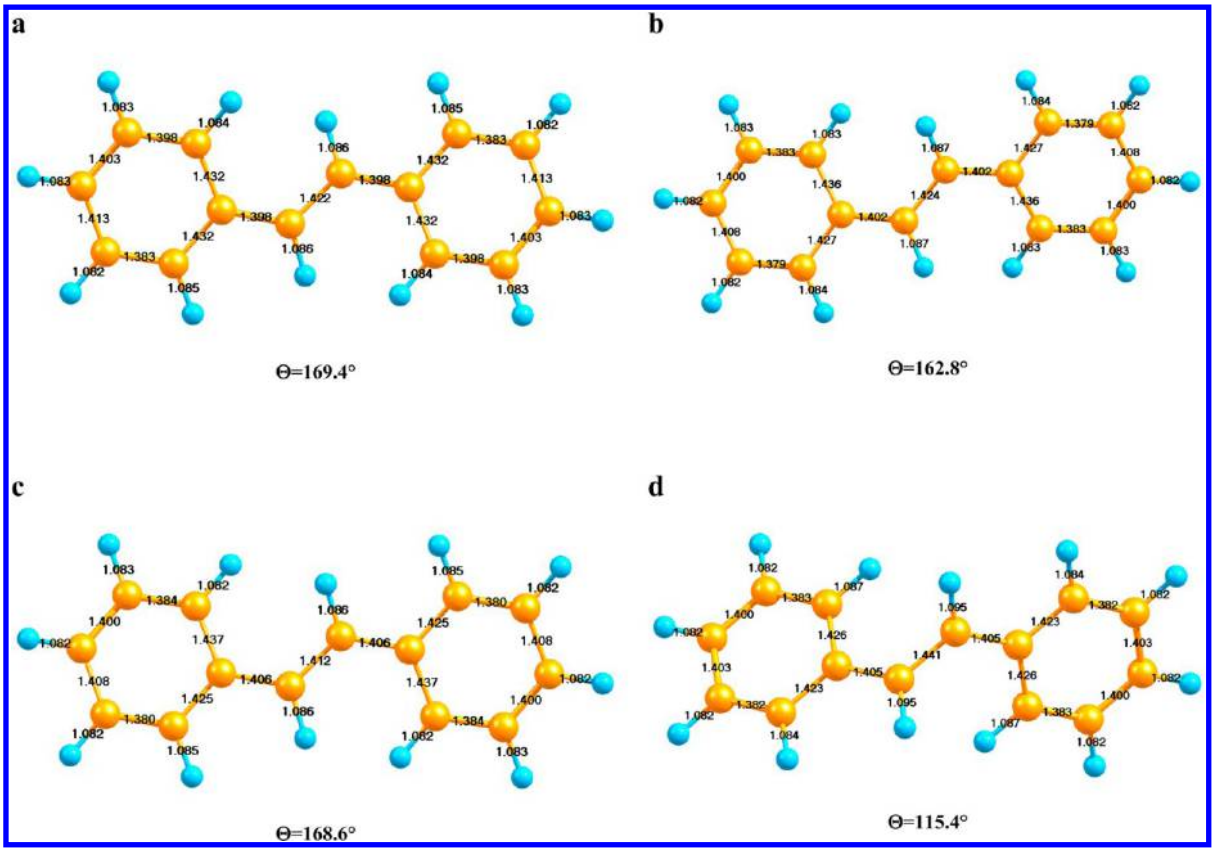

Figure 5. Optimized S_1 state of *trans*-stilbene: (a) SA2-XMCQDPT2(10,10) (averaging over the two lowest *B* states); (b) SA3-XMCQDPT2(2,2); (c) pure state XMCQDPT2(2,2); and (d) trans-to-cis isomerization barrier, SA3-XMCQDPT2(2,2). Dihedral twisting angles at the central ethylenic bond are indicated.

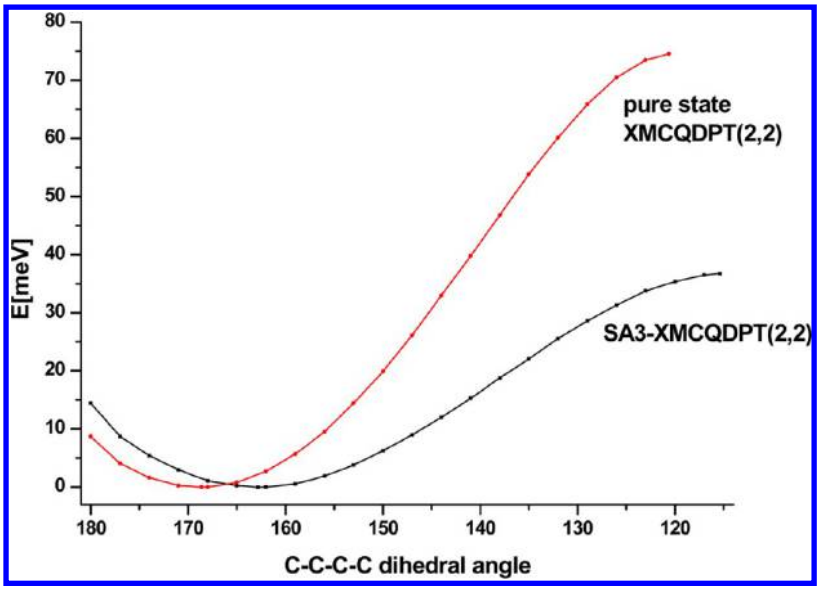

Figure 6. Relaxed PES scans along the twisting coordinate in the S_1 state in *trans*-stilbene.

The three optimized geometries of the S_1 state in *trans*-stilbene are shown in Figure 5. In all three structures one finds good agreement in the optimized bond lengths. However a difference appears in the central dihedral angle: SA3-XMCQDPT2(2,2) predicts somewhat higher twisting than pure-state and XMCQDPT2(10,10) calculations. In the latter case it is not an effect of omitting the *A*-states from averaging, since virtually the same geometry is observed with SA6- and SA5-optimizations when the said states are included. All of the above levels of theory predict nonplanarity of the stationary point but, in contrast with the ground state, this is due to the central dihedral angle, i.e. the photoisomerizational twisting coordinate, while the benzene rings are now in plane with the weakened central bond.

Relaxed PES scans along the twisting coordinate from the planar C_{2h} geometry to the optimized trans-to-cis isomerization

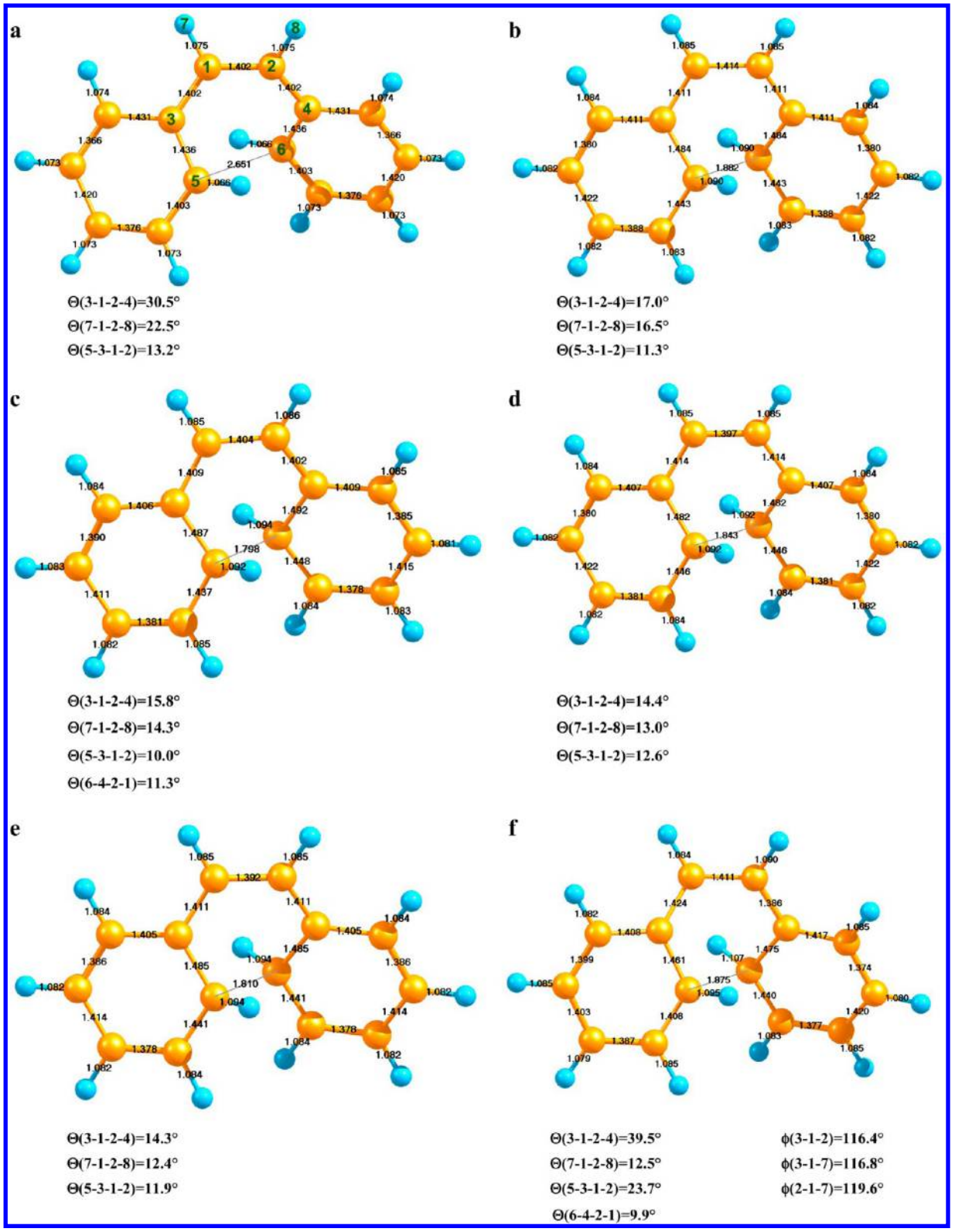

Figure 7. Important geometric points in the DHP geometric domain: (a) SA3-CASSCF(14,14) *cis*-stilbenic minimum; (b) optimized S_1, SA2-XMCQDPT2(10,10); (c) optimized S_1, SA3-XMCQDPT2(2,2); (d) optimized S_2, pure state XMCQDPT2(10,10); (e) optimized S_2, SA3-XMCQDPT2(2,2); (f) intersection point of S_0/S_1, SA3-XMCQDPT2(2,2). See (a) for atom numbering.

barrier (**TS1** of Figure 4 and Table 2) are shown in Figure 6. Similarly to the ground state, the barrier between the equivalent C_2-minima that differ in the direction of twisting around the central ethylenic bond is quite low. With regard to the isomerization barrier, the pure state XMCQDPT2(2,2) calculation predicts a higher value of 75 meV. Unfortunately we encountered technical difficulties in optimizing the saddle point at the XMCQDPT2(10,10) level, but the almost converged energy and the value of the twisting angle are remarkably close to the pure state XMCQDPT2(2,2) data.

dx.doi.org/10.1021/ct400647w | *J. Chem. Theory Comput.* 2013, 9, 4973−4990

Single-point SA6-XMCQDPT2(14,14) recalculations of the barrier height gave an increase to 52 meV for SA3-XMCQDPT2(2,2) geometries and a decrease to 65 meV for the pure state ones. Thus, the experimental barrier height of ca. 0.15 eV[2,5,6,9,31] could not be confirmed by the XMCQDPT2 theory, at least as far as additional expansion of the active space with σ-orbitals is computationally unbearable. Leitner et al.[100] demonstrated that higher barrier heights, in better agreement with experiments, may be obtained at the SA5-CASSCF(14,12) level. Indeed, our own C_2-constrained SA3-CASSCF(14,14) results yielded a value of above 0.3 eV. Thus, the PT2 dynamic correlation contributions seem to overcorrect the overestimated CASSCF barrier heights. The best theoretical approximation to the experimental results so far belongs to the SF-TDDFT (BHHLYP).[129]

In view of the fact that after passing the trans-to-cis isomerization barrier the molecule undergoes spontaneous pyramidalization, we undertook a search for potential symmetry-unconstrained transition states near the constructed symmetric MEP of the S_1 state. A series of SA3-XMCQDPT-(2,2) geometry optimizations were performed with increasing fixed values of out-of-plane bending of one of the central C−H bonds in order to locate possible low lying C_1 configurations. The said optimizations were launched both from the vicinity of the stationary point of S_1 and from the vicinity of the located isomerization barrier. In no case any indication of low lying asymmetric transition states was observed. It may be therefore concluded that the increased isomerization rate of *trans*-stilbene in some solvents[55] is not associated with activation of any new pathways other than the conventional C_2-symmetric twisting by the dynamically asymmetric solvent environment. Recently, a new model based on solute−solvent collisions has been proposed to rationalize the solvent dependence of the isomerization rate.[58]

In our previous work,[57] we reported SA3-XMCQDPT2(2,2) vibrational calculations for the stationary point of *trans*-S_1 (see SI). Now we complemented them with the similar calculations for the optimized transition state. In the comprehensive LMRT-RRKM study of the *trans*-stilbene case,[100] the transition-state frequencies were calculated explicitly rather than assumed from the stationary point as in the earlier studies. The CASSCF frequency for the reaction coordinate was reported to be about 600 cm^{-1} for the nondeuterated molecule. We cannot corroborate their result; our calculation predicts the reaction frequency at about 30 cm^{-1}, both the real one at the stationary point and the imaginary one at the transition state, in good agreement with analogous SF-TDDFT predictions.[129] Taking into account that after further 2−3° of twisting past the transition state there already occurs spontaneous pyramidalization of one of the central ethylenic carbon atoms, while the *trans*-S_1 minimum is rather stable with respect to out-of-plane C−H bending, it is to be expected that a number of vibrational frequencies change upon going from the minimum to the transition state. Indeed, we found that the zero point vibrational correction (ZPE) to the barrier height is −42 meV or ca. −340 cm^{-1}, a value which is not attributable to a particular vibration but rather distributed between different modes. Thus, the vibrational correction effectively cancels out the PES-based barrier value obtained at the SA3-XMCQDPT2(2,2) level, which points to a need of high-level treatment of anharmonic effects for reliable theoretical rationalization of vibrational properties of the excited *trans*-stilbene. Interestingly, despite the differences in the vibrational frequencies, the temperature dependence of the Gibbs energy of activation was found to be totally negligible (unlike that of the activation enthalpy, however), and the kinetics of isomerization is therefore determined by the ZPE contribution.

The zero-point corrections made it possible to rationalize the well-known kinetic isotope effect in the isomerization of deuterated *trans*-stilbene: no changes upon D_{10} substitution at the phenyl rings but a 1.4-fold decrease in the rate for the D_2 substitution at central ethylenic carbons and 1.5-fold decrease for the complete D_{12} substitution[31] (gas phase experiments with varied amount of vibrational excitation give the ratio of 1.6−1.8[6]). We calculate that D_2- and D_{12}-substitutions increase the ZPE-corrected barrier (as well as $G^{\ddagger}(298)$) by ca. 10 meV, which translates into a factor of ca. 1.5 in reaction rate at room temperature, in good agreement with the experimental data, while the D_{10}-substitution at the phenyl rings has virtually no effect on the barrier at all. A similar numerical conclusion was reached by Leitner et al.,[100] but that was largely based on hugely overestimated and deuteration-dependent reaction coordinate frequency.

Excited *cis*-Stilbene, the DHP Domain of S_1, and Insight into Cis-to-Trans Isomerization. Our results on *cis*-silbene perfectly corroborated the suggestion[129] that the truly *cis*-stilbenic rather than DHP-like stationary point in S_1 can be predicted by methods that lack dynamic correlation, like CASSCF(2,2),[99] but not by the approaches that include it. As mentioned earlier, we have located the *cis*-stilbenic stationary point at the CASSCF level even with the (14,14) active space (see Figure 7). However the XMCQDPT2 calculations do not confirm the CASSCF results. Even in the C_2-constrained computation we observe only a decrease in steepness of the PES in a certain region of geometries rather than the presence of a symmetry-constrained stationary point. To ensure that nothing is being missed, we performed SA5- and SA6-XMCQDPT2(10,10) optimizations starting both from the geometry of the *cis*-stilbene ground state and from the CASSCF(14,14) stationary point of S_1 and obtained similar results (see Figure 7).

When the DHP geometry is being approached starting from *cis*-stilbene, the HOMO and the LUMO acquire a degree of, respectively, σ-antibonding and σ-bonding character with respect to the emerging bond between the phenyl rings. This causes an interplay between the increasing σ-bonding and the decreasing integral degree of π-bonding upon HOMO−LUMO transitions. The σ-bonding effects are modest, as they come at a cost of breaking the aromaticity of the phenyls and steric strains in DHP. As a result, while S_1 near the CASSCF(14,14) *cis*-stilbenic stationary point is a result of single HOMO−LUMO excitation of B symmetry no less than 2.7 eV above S_0 and 0.6−0.7 eV below the higher excited states, in the DHP region the B-symmetric state and the two A states (the latter being dominated by the linear combinations of $HOMO^2LUMO^0$ and $HOMO^0LUMO^2$ configurations) form a much closer spaced S_0−S_2 manifold within a range of less than 1.2 eV and are separated from the higher excited states by further 1.2 eV or ,pre. With regard to details, we observe here a minor discrepancy between the XMCQDPT2(10,10) and the SA3-XMCQDPT2(2,2) predictions. XMCQDPT2(10,10) with various state-averaging schemes predicts the A state to become S_1 and the B state to be S_2, both states having rather similar symmetric stationary points. SP-SA6-XMCQDPT2(14,14) recalculations for the S_1 optimized with averaging over the two lowest A states and for pure state-optimized S_2 predict the

separation of their minima to be 374 meV. At the SA3-XMCQDPT2(2,2) level, however, the two excited states interact, which results in a stationary point in S_1 that loses symmetry. Nevertheless, with the weight of the single HOMO−LUMO excitation below 0.1, the relation of S_1 to the A state is apparent. S_2 is obtained, similarly to XMCQDPT2(10,10), as a perfectly C_2-symmetric HO-MO^{1}LUMO^1 B state, its stationary point being located 354 meV above that of S_1.

In Figure 7, we present the geometry of all stationary points in S_1 and S_2 thus located. The SA3-XMCQDPT2(2,2) minimum energy clossing point of S_0/S_1 (also Figure 7; known as "ring cooperation intersection"[94,129]) is located 403 meV above the stationary point of S_1—much higher than predicted by SF-TDDFT.[129] This point is characterized by pyramidalization of one of the ethylenic carbons, though it much less pronounced than in the pyramidalized domain of S_1. SP-SA6-XMCQDPT2(14,14) recalculation at the crossing point gives a separation of 114 meV between S_0 and S_1; this can be regarded as a rather good agreement. The average of the XMCQDPT2(14,14) energies of S_0 and S_1 at the crossing point is 395 meV above the DHP-like minimum of S_1.

The twisting dihedral angle that we used, for the purpose of uniformity of our description, as an optimization constraint throughout all the principal geometric domains (as was shown in Figure 4) is not, in fact, the most appropriate coordinate for studying the PES in the DHP domain. When the relaxed scan of the PES along the twisting angle is performed, the major changes are mostly restricted to the central bridging unit of the molecule while the relative positions of the phenyl moieties show rather limited variation. Therefore a more natural choice for the scanned coordinate is the distance between the phenyl ring carbon atoms that are linked in DHP. The relaxed scan of S_1 (and also of S_2 in the region where it remains a locally stable B-symmetric state) along the C···C distance in question is shown in Figure 8. For S_1, one can see the two disjoint scan paths with a small overlapping region where both are locally stable: the "parabolic" section at shorter C···C separations belongs to the nonsymmetric S_1 state dominated by the closed-shell HOMO^{2}LUMO^0 and HOMO^{0}LUMO^2 configurations; above it one can find the C_2-symmetric (B) HOMO^{1}LUMO^1

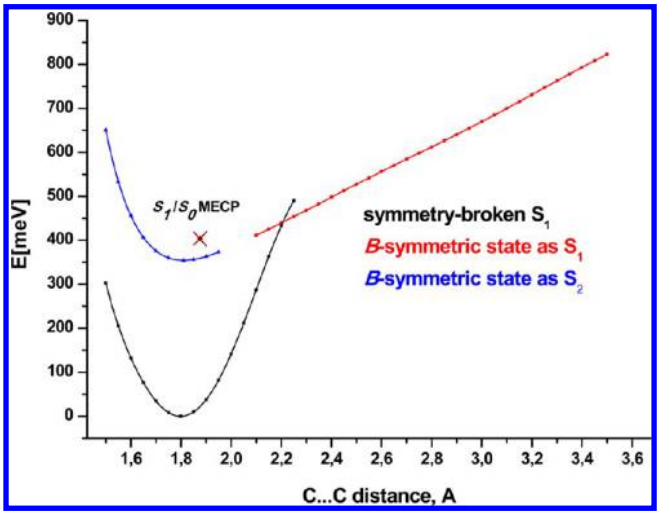

Figure 8. Relaxed scans of the S_1 and S_2 in the DHP/*cis*-stilbene region along the distance between the phenyl carbon atoms that are linked in DHP.

S_2. At higher separations the B state becomes S_1 and its geometry turns increasingly *cis*-stilbenic, i.e. lacking pyramidalization of the carbon atoms in question. We found that the depth of the potential well in S_2 is within 30 meV and at C···C separations beyond 1.95 Å direct relaxation into S_1 is possible through an intersection of the two states. Thus, while it is S_2 that is related by symmetry to the initially excited *cis*-stilbene, its population exchange with S_1 must be extremely rapid.

Summarizing our findings for the DHP/*cis*-stilbene side of the potential energy surface, we conclude that initial excitation of *cis*-stilbene, vertical or nearly vertical, brings it to a state which is strongly separated from any stationary point, both in terms of geometry and energy, which results in a considerable amount of vibrational excitation (see Figure 4). Hence the photoisomerization of *cis*-stilbene is hardly describable in quasi-thermodynamic terms; it is rather a dynamic problem that involves a complex manifold of electronic states, the driving force for isomerization being the energy gradient in the S_1 state toward higher twisting angles, and the passage of the excited *cis*-stilbene into the pyramidalized state is effectively barrierless. We have already presented some experimental evidence in favor of this conclusion in our previous work on the resonant Raman spectra of excited stilbene;[57] earlier, continuous evolution of the excited *cis*-stilbene was also shown by means of transient impulsive Raman technique.[52] Although some experimental studies suggest a shallow barrier to account for a lifetime of an order of 1 ps,[23,34,53−55] this may be a mere consequence of the formal kinetic treatment of the spectroscopic data. Even conjecturing transient stability of the *cis*-stilbenic rather than DHP geometry in S_1 and considering the effective barrier for its transformation into the phantom state, the respective estimate will exceed 0.1 eV.

The observed partial conversion into DHP may involve a faster cooling portion of excited molecules that become thus trapped in the DHP potential well. Unfortunately, performing dynamic simulations with XMCQDPT2 potentials and appropriate sampling is presently out of question due to extremely costly numerical gradients while lower-quality potentials can hardly allow for quantitatively reliable conclusions. One can mention, however, a series of works where the semiclassical SERID approach was applied to dynamics of both *cis*- and *trans*-stilbene.[120−125]

Pyramidalized (Phantom) State. The pyramidalized, nonsymmetric (C_1) domain of the PES of the S_1 state, where the S_0/S_1 intersection responsible for the ultimate relaxation and for trans−cis branching is located, has been already described both at the CASSCF (also with CASPT2 recalculations)[99] and SF-TDDFT[129] levels. The principal geometric features of this domain, as revealed by our calculations, are as follows: only one of the central ethylenic carbons is considerably pyramidalized, and the rotation of the adjacent phenyl group is tightly connected with the orientation of the π-orbital axis or the C—H bond at the said ethylenic center. The second ethylenic carbon atom remains, to the contrary, almost perfectly planar, its phenyl substituent being in-plane with the central C═C bond. Such pyramidalization has been already computationally described in hexatriene,[150,151] a simpler symmetric conjugated system with isomerization around the ethylenic double bond and in the ethylene itself.[99,102]

The key geometries obtained in the present work are shown in Figure 9. The main difference between the stationary point geometries optimized at the SA3-XMCQDPT(2,2) and SA2-

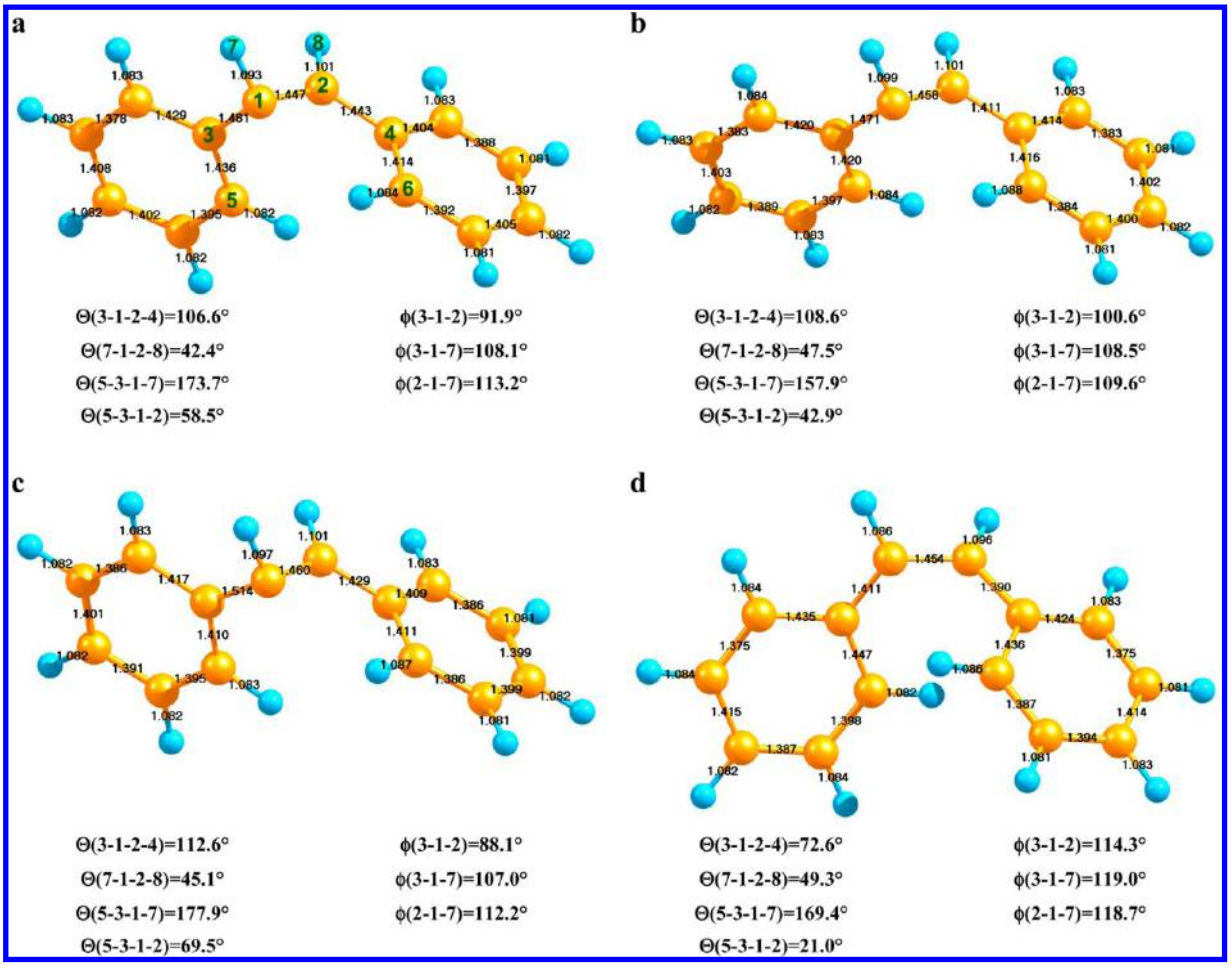

Figure 9. Important geometric points in the pyramidalized domain of S_1: (a) optimized energy minimum, SA2-XMCQDPT(10,10); (b) optimized energy minimum, SA3-XMCQDPT(2,2); (c) S_1/S_0 intersection, SA3-XMCQDPT(2,2); (d) pyramidalized-to-DHP transition state, SA3-XMCQDPT(2,2). See (a) for atom numbering.

XMCQDPT(10,10) levels consists in the orientation of the phenyl ring at the pyramidalized carbon: calculation with the minimum active space predicts it to be approximately perpendicular to the axis of the π-orbital on the said carbon, whereas with the (10,10) space the ring turns more in-plane with the C−H bond and generally changes the geometric parameters closer to the S_1/S_0 crossing point. Note that XMCQDPT(10,10) calculations become quite sensitive to the state-averaging scheme: in particular, the SA6 variant fully merges the minimum with the S_1/S_0 minimum energy crossing point, whereas the SA3-XMCQDPT(2,2) and SA2-XMCQDPT(10,10) optimizations, as well as sp-SA6-XMCQDPT2(14,14) recalculation, predict a distinct energy minimum with a gap to S_0 between 0.4 and 0.6 eV. Importantly, both the stationary point and the S_0/S_1 intersection are quite far from the trans−cis transition barrier in S_0, in terms of both energy and geometry: the latter is located 0.9−1.1 eV lower depending on the active space and averaging scheme employed.

Pyramidalization of the ethylenic carbon in the direction opposite to that shown in Figure 9 was also checked, and turns out to be totally unfavorable. This is possibly due to shortening of the distance between the two hydrogen atoms bearing small effective positive charges: the one at the pyramidalized carbon atom and another one in the opposite phenyl fragment. Asymmetry of the electronic states results in considerable polarity of the S_1. While its dipole moment does not exceed 1 D in the *trans*-stilbene and 2 D in the somewhat symmetry broken DHP domain, it reaches 9 D in a pyramidalized molecule, comparable to the SF-TDDFT value of 8 D.[129] It is noteworthy that the charge separation is largely confined in the central ethylenic unit: the Löwdin charge of the pyramidalized carbon atom **1** (hereinafter hydrogen atoms included) is as high as −0.41 and that of its planar neighbor **2** equals +0.37 while their adjacent phenyl moieties bear integral charge of −0.24 and +0.28, respectively. However, in the smaller hexatriene that lacks aromatic conjugation of stilbene, pyramidalization is similar geometrically but not in terms of charge distribution, being associated with "radicalization" of the respective carbon atoms rather than with sudden polarization.[151]

Quite important for the issues of excited state dynamics is the degree of correlation between the twisting and pyramidalization coordinates. While in the SF-TDDFT survey[129] this was directly addressed by means of 2D PES scans, in our case that was too expensive. However, even our 1D scans enable us to conclude that the two coordinates correlate tightly. This is illustrated by Figure 10 where we plot the relations between twisting and pyramidalization (measured by out-of-plane C−H bending at the pyramidalized center) for the separate relaxed scans along these two coordinates. As one can see, the two curves diverge only moderately. Note that for the scan along the twisting coordinate, changes of the H−C−C−H dihedral angle at the central ethylenic bond are marginal and remain

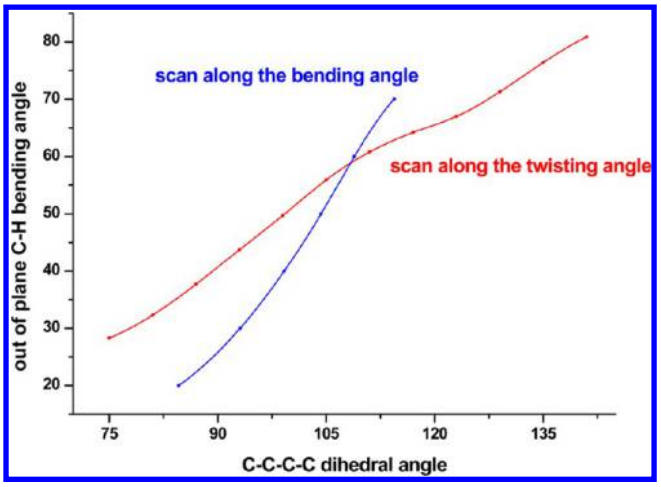

Figure 10. Relation between the C−C−C−C twisting angle at the central ethylenic bond and out-of-plane C−H bending at the pyramidalized ethylenic carbon for the S_1 PES scans along the twisting and bending coordinates.

within the range of 47−53°. The changes in this angle along the bending coordinate are, however, more pronounced.

CASSCF(2,2) and CASPT2 calculations by Quenneville and Martinez demonstrated that the gradient of S_0 near the S_0/S_1 intersection region is considerably higher than that of S_1.[99] This result is supported by our findings: the minimum energy crossing point was found only 6 meV above the stationary point of the pyramidalized domain at the SA3-XMCQDPT2(2,2) level, the respective geometry changes being associated with further pyramidalization toward the crossing point. Being much lower than the 130 meV SF-TDDFT estimate[129] and not far from the MS-CASPT2(2,2) prediction that the intersection point constitutes the very minimum on the PES,[102] our value seems to be in best agreement with the experimental observation of the short-lived phantom state[55] before recovery of the ground state. For this intersection, we have a less good agreement with SP-SA6-XMCQDPT2(14,14) recalculation, which yielded an S_0-S_1 gap of 270 meV. We regard this as an effect of high ground state gradient coupled with expectable differences in optimal geometries upon variation of the active space and introduction of the ISA shift.

Attempts to locate a C_2-symmetric S_0/S_1 intersection point failed both at the CASSCF and XMCQDPT2 levels. There always remains a considerable gap between the two states, and pyramidalization of the central ethylenic carbons must, therefore, play a vital role in photoisomerization of *cis*-stilbene no less than for the *trans*-isomer. Possibly, the real picture will be close to the "hula-twist" mechanism suggested by Fuss et al.,[47] and there might even be some kinetic isotope effect of dynamic nature.

In view of the lack of symmetry of the perpendicular state geometry, quite intriguing are the comparable yields of the ground state trans- and the cis-products upon photoisomerization of either of them.[64,71,73] As one can see, the C−C−C−C twisting angle in the stationary point of S_1 and the S_0/S_1 intersection point is somewhat on the trans side; the more cis-like H−C−C−H dihedral angle will be of lower importance due to higher velocities of hydrogen atoms. The positions of the bulky phenyl rings also seem to slightly favor the transformation into the *trans*-stilbene. However, the excited wavepackets that arrive to the perpendicular state likely keep a certain amount of internal energy to be distributed over a quite a range of twisting and phenyl rotation angles near the stationary point. Therefore, we cannot currently provide reliable means to model the trans−cis branching quantitatively while retaining sufficiently high nonempirical quality of the electronic potential. However, to obtain a qualitative picture, we carried out two SA3-XMCQDPT2(2,2) calculations on S_0 starting from the close vicinity of the S_0/S_1 intersection point: a fully relaxed intrinsic reaction coordinate (IRC) scan and an energy conserved dynamic reaction coordinate (DRC) scan. While the position of phenyl rings remained the slowest part of the evolution, the configuration of the central bridging unit experienced rapid transformation into the cis configuration in case of IRC and trans configuration for DRC. One can thus expect that intermediate range of energy dissipation rates may, indeed, afford the observed comparable yield of *cis*- and *trans*-stilbene.

CONCLUSIONS

XMCQDPT2 may now gradually become a new powerful ab initio tool for studying excited electronic states beyond the level of single point recalculations. This was demonstrated with the S_1 state of stilbene. In this case, many experimental observations exist related to photoisomerization, and the ability to reproduce or explain them computationally may serve as an indicator for the predictive quality of the method. Even though errors on the order of 0.1 eV remain for problematic quantities like heights of activation barriers, second-order quasi-degenerate perturbation theories are still second to none in studying excited states of medium-sized molecules. As could be seen for *cis*-stilbene, XMCQDPT2 corrects serious qualitative mistakes of the CASSCF description. While the TDDFT alternatives are computationally cheaper, their reliability in each particular case will always be questionable, so XMCQDPT2 verification will never be useless. In the stilbene case, we see good qualitative agreement with the previous LR-TDDFT and SF-TDDFT results, which suggests that the basic facts are clarified and these are quantitative details that can be further improved, though some may require the level of molecular dynamics treatments, which is not available at present.

Stilbene, in its turn, constitutes an interesting object for methodological studies of the capabilities of XMCQDPT2 in terms of selection of better performing zero order Hamiltonians, optimal ISA shifts, etc. The (14,14) size of the π-electron active space can readily be found in systems of practical importance while still remaining within the reach of the modern quantum chemical software Especially interesting is the possibility of description of the S_1 state using only the minimum active space and mostly without the use of the ISA shifts. With quite an amount of high quality experimental data available, such as the trans-to-cis isomerization barrier, one can find a convenient test case for fine-tuning of the details of PT2 computational approaches.

ASSOCIATED CONTENT

Supporting Information

Cartesian coordinates of the key geometries mentioned and depicted in the text; harmonic vibrational frequencies of excited *trans*-stilbene in the energy minimum and transition state and reaction coordinate at transition state. This material is available free of charge via the Internet at http://pubs.acs.org.

AUTHOR INFORMATION

Corresponding Authors

*E-mail: ioffe@phys.chem.msu.ru.
*E-mail: alex.granovsky@gmail.com.

Author Contributions

The manuscript was written through equal contributions of both authors. Both authors have given approval to the final version of the manuscript.

Notes

The authors declare no competing financial interest.

ACKNOWLEDGMENTS

We are deeply grateful to Prof. N. P. Ernsting, Dr. S. A. Kovalenko, and Dr. A. L. Dobryakov (HU Berlin) for invaluable discussions and comments and to the Moscow State University supercomputer center for access to "Lomonosov" and "Chebyshev" supercomputers and strong computational support.[152] A.A.G. is grateful to RFBR for financial support through Grant No. 11-03-01214.

ABBREVIATIONS

CAS, complete active space; PT2, second-order perturbation theory; MS, multistate; MR, multireference; QD, quasi-degenerate; SP, single-point; XMCQDPT2, extended multi-configuration quasi-degenerate PT2; SA, state-averaged; CASSCF, complete active space SCF; CASCI, complete active space configuration interaction; CASPT2, complete active space PT2; XMS-CASPT2, extended multistate CASPT2; NEVPT2, N-electron valence PT2; MP2, second-order Möller−Plesset perturbation theory; MP4(SDQ), fourth-order Möller−Plesset perturbation theory with single, double, and quadruple excitations; IVO, improved virtual orbital; IVO-MRMP, IVO Möller−Plesset perturbation theory; DFT, density functional theory; TDDFT, time-dependent DFT; LR-TDDFT, linear response TDDFT; SF-TDDFT, spin-flip TDDFT; PJTE, pseudo-Jahn−Teller effect; PES, potential energy surface; MEP, minimum energy path; MECP, minimum energy crossing point; HOMO, highest occupied molecular orbital; LUMO, lowest unoccupied molecular orbital; DHP, 4a,4b-dihydrophenanthrene

REFERENCES

(1) Liu, F.; Morokuma, K. *J. Am. Chem. Soc.* **2012**, *134*, 4864−4876.
(2) Syage, J. A.; Lambert, W. R.; Felker, P. M.; Zewail, A. H.; Hochstrasser, R. M. *Chem. Phys. Lett.* **1982**, *88*, 266−270.
(3) Perry, J. W.; Scherer, N. F.; Zewail, A. H. *Chem. Phys. Lett.* **1983**, *103*, 1−8.
(4) Syage, J. A.; Felker, P. M.; Zewail, A. H. *J. Chem. Phys.* **1984**, *81*, 4685−4705.
(5) Syage, J. A.; Felker, P. M.; Zewail, A. H. *J. Chem. Phys.* **1984**, *81*, 4706−4723.
(6) Felker, P. M.; Zewail, A. H. *J. Phys. Chem.* **1985**, *89*, 5402−5411.
(7) Felker, P. M.; Lambert, W. R.; Zewail, A. H. *J. Chem. Phys.* **1985**, *82*, 3003−3010.
(8) Pedersen, S.; Bañares, L.; Zewail, A. H. *J. Chem. Phys.* **1992**, *97*, 8801−8804.
(9) Heikal, A. A.; Chong, S. H.; Baskin, J. S.; Zewail, A. H. *Chem. Phys. Lett.* **1995**, *242*, 380−389.
(10) Baumert, T.; Frohnmeyer, T.; Kiefer, B.; Niklaus, P.; Strehle, M.; Gerber, G.; Zewail, A. H. *Appl. Phys. B: Laser Opt.* **2001**, *72*, 105−108.
(11) Greene, B. I.; Hochstrasser, R. M.; Weisman, R. B. *J. Chem. Phys.* **1979**, *71*, 544−545.
(12) Greene, B. I.; Hochstrasser, R. M.; Weisman, R. B. *Chem. Phys.* **1980**, *48*, 289−298.
(13) Rothenberger, G.; Negus, D. K.; Hochstrasser, R. M. *J. Chem. Phys.* **1983**, *79*, 5360−5367.
(14) Negus, D.K..; Green, D.S..; Hochstrasser, R. M. *Chem. Phys. Lett.* **1985**, *117*, 409−413.
(15) Lee, M.; Holtom, G. R.; Hochstrasser, R. M. *Chem. Phys. Lett.* **1985**, *118*, 359−363.
(16) Myers, A. B.; Holt, P. I.; Pereira, M. A.; Hochstrasser, R. M. *Chem. Phys. Lett.* **1986**, *132*, 585−590.
(17) Abrash, S.; Repinec, S. T.; Hochstrasser, R. M. *J. Chem. Phys.* **1990**, *93*, 1041−1053.
(18) Sension, R. J.; Repinec, S. T.; Hochstrasser, R. M. *J. Phys. Chem.* **1991**, *95*, 2946−2948.
(19) Repinec, S. T.; Sension, R. J.; Szarka, A. Z.; Hochstrasser, R. M. *J. Phys. Chem.* **1991**, *95*, 10380−10385.
(20) Sension, R. J.; Szarka, A. Z.; Hochstrasser, R. M. *J. Chem. Phys.* **1992**, *97*, 5239−5242.
(21) Sension, R. J.; Repinec, S. T.; Szarka, A. Z.; Hochstrasser, R. M. *J. Chem. Phys.* **1993**, *98*, 6291−6315.
(22) Schroeder, J.; Schwarzer, D.; Troe, J.; Voss, F. *J. Chem. Phys.* **1990**, *93*, 2392−2404.
(23) Nikowa, L.; Schwarzer, D.; Troe, J.; Schroeder, J. *J. Chem. Phys.* **1992**, *97*, 4827−4835.
(24) Schroeder, J.; Troe, J.; Vohringer, P. *J. Chem. Phys. Lett.* **1993**, *203*, 255−260.
(25) Schroeder, J.; Schwarzer, D.; Troe, J.; Vohringer, P. *J. Chem. Phys. Lett.* **1994**, *218*, 43−50.
(26) Nikowa, L.; Schwarzer, D.; Troe, J. *Chem. Phys. Lett.* **1995**, *233*, 303−308.
(27) Meyer, A.; Schroeder, J.; Troe, J.; Votsmeier, M. *J. Photochem. Photobiol A* **1997**, *105*, 345−352.
(28) Meyer, A.; Schroeder, J.; Troe, J. *J. Phys. Chem. A* **1999**, *103*, 10528−10539.
(29) Courtney, S. H.; Fleming, G. R. *J. Chem. Phys.* **1985**, *83*, 215−222.
(30) Balk, M. W.; Fleming, G. R. *J. Phys. Chem.* **1986**, *90*, 3975−3983.
(31) Courtney, S. H.; Balk, M. W.; Philips, L. A.; Webb, S. P.; Yang, D.; Levy, D. H.; Fleming, G. R. *J. Chem. Phys.* **1988**, *89*, 6697−6707.
(32) Todd, D. C.; Jean, J. M.; Rosenthal, S. J.; Ruggiero, A. J.; Yang, D.; Fleming, G. R. *J. Chem. Phys.* **1990**, *93*, 8658−8668.
(33) Todd, D. C.; Fleming, G. R.; Jean, J. M. *J. Chem. Phys.* **1992**, *97*, 8915−8925.
(34) Todd, D. C.; Fleming, G. R. *J. Chem. Phys.* **1993**, *98*, 269−279.
(35) Sumitani, M.; Nakashima, N.; Yoshihara, K.; Nagakura, S. *Chem. Phys. Lett.* **1977**, *51*, 183−185.
(36) Teschke, O.; Ippen, E. P.; Holtom, G. R. *Chem. Phys. Lett.* **1977**, *52*, 233−235.
(37) Taylor, J. R.; Adams, M. C.; Sibbett, W. *Appl. Phys. Lett.* **1979**, *35*, 590−592.
(38) Heisel, F.; Miehe, J. A.; Sipp, B. *Chem. Phys. Lett.* **1979**, *61*, 115−118.
(39) Amirav, A.; Jortner, J. *Chem. Phys. Lett.* **1983**, *95*, 295−300.
(40) Zwier, T. S.; Carrasquillo, M. E.; Levy, D. H. *J. Chem. Phys.* **1983**, *78*, 5493−5505.
(41) Spangler, L. H.; Van Zee, R.; Zwier, T. S. *J. Phys. Chem.* **1987**, *91*, 2782−2786.
(42) Spangler, L. H.; Vanzee, R. D.; Blankespoor, S. C.; Zwier, T. S. *J. Phys. Chem.* **1987**, *91*, 6087−6089.
(43) Suzuki, T.; Mikami, M.; Ito, M. *J. Phys. Chem.* **1986**, *90*, 6431−6440.
(44) Sundström, V.; Gillbro, T. *Chem. Phys. Lett.* **1984**, *109*, 538−543.
(45) Warmuth, C.; Milota, F.; Kauffmann, H. F.; Wadi, H.; Pollak, E. *J. Chem. Phys.* **2000**, *112*, 3938−3941.
(46) Fuss, W.; Kosmidis, C.; Schmid, W. E.; Trushin, S. A. *Chem. Phys. Lett.* **2004**, *385*, 423−430.

(47) Fuss, W.; Kosmidis, C.; Schmid, W. E.; Trushin, S. A. *Angew. Chem., Int. Ed.* **2004**, *43*, 4178−4182.
(48) Takeuchi, S.; Tahara, T. *Chem. Phys. Lett.* **2000**, *326*, 430−438.
(49) Ishii, K.; Takeuchi, S.; Tahara, T. *Chem. Phys. Lett.* **2004**, *398*, 400−406.
(50) Ishii, K.; Takeuchi, S.; Tahara, T. *J. Phys. Chem. A* **2008**, *112*, 2219−2227.
(51) Nakamura, T.; Takeuchi, S.; Suzuki, N.; Tahara, T. *Chem. Phys. Lett.* **2008**, *465*, 212−215.
(52) Takeuchi, S.; Ruhman, S.; Tsuneda, T.; Chiba, M.; Taketsugu, T.; Tahara, T. *Science* **2008**, *322*, 1073−1077.
(53) Nakamura, T.; Takeuchi, S.; Taketsugu, T.; Tahara, T. *Phys. Chem. Chem. Phys.* **2012**, *14*, 6225−6232.
(54) Sajadi, M.; Dobryakov, A. L.; Garbin, E.; Ernsting, N. P.; Kovalenko, S. A. *Chem. Phys. Lett.* **2010**, *489*, 44−47.
(55) Kovalenko, S. A.; Dobryakov, A. L.; Ioffe, I.; Ernsting, N. P. *Chem. Phys. Lett.* **2010**, *493*, 255−258.
(56) Weigel, A.; Ernsting, N. P. *J. Phys. Chem. B* **2010**, *114*, 7879−7893.
(57) Dobryakov, A. L.; Ioffe, I.; Granovsky, A. A.; Ernsting, N. P.; Kovalenko, S. A. *J. Chem. Phys.* **2012**, *137*, 244505.
(58) Kovalenko, S. A.; Dobryakov, A. L. *Chem. Phys. Lett.* **2013**, *570*, 56−60.
(59) Kovalenko, S. A.; Dobryakov, A. L.; Pollak, E.; Ernsting, N. P. *J. Chem. Phys.* **2013**, *139*, 011101.
(60) Greene, B. I.; Farrow, R. C. *J. Chem. Phys.* **1983**, *78*, 3336−3338.
(61) Saltiel, J. *J. Am. Chem. Soc.* **1967**, *89*, 1036−1037.
(62) Saltiel, J.; D'Agostino, J. T. *J. Am. Chem. Soc.* **1972**, *94*, 6445−6456.
(63) Saltiel, J.; Waller, A. S.; Sun, Y.-P.; Sears, D. F., Jr. *J. Am. Chem. Soc.* **1990**, *112*, 4580−4581.
(64) Saltiel, J.; Waller, A. S.; Sears, D. F., Jr. *J. Photochem. Photobiol A.* **1992**, *65*, 29−40.
(65) Saltiel, J.; Waller, A. S.; Sears, D. F., Jr. *J. Am. Chem. Soc.* **1993**, *115*, 2453−2465.
(66) Myers, A. B.; Mathies, R. A. *J. Chem. Phys.* **1984**, *81*, 1552−1558.
(67) Myers, A. B.; Trulson, M. O.; Mathies, R. A. *J. Chem. Phys.* **1985**, *83*, 5000−5006.
(68) Ci, X.; Myers, A. B. *Chem. Phys. Lett.* **1989**, *158*, 263−270.
(69) Rodier, J. M.; Ci, X. P.; Myers, A. B. *Chem. Phys. Lett.* **1991**, *183*, 55−62.
(70) Phillips, D. L.; Rodier, J. M.; Myers, A. B. *Chem. Phys.* **1993**, *175*, 1−12.
(71) Rodier, J. M.; Myers, A. B. *J. Am. Chem. Soc.* **1993**, *115*, 10791−10795.
(72) Urano, T.; Hamaguchi, H.; Tasumi, M.; Yamanouchi, K.; Tsuchiya, S.; Gustafson, T. L. *J. Chem. Phys.* **1989**, *91*, 3884−3894.
(73) Petek, H.; Yoshihara, K.; Fujiwara, Y.; Frey, J. G. *J. Opt. Soc. Am. B* **1990**, *7*, 1540−1544.
(74) Champagne, B. B.; Pfanstiel, J. P.; Plusquellic, D. F.; Pratt, D. W.; Van Herpen, W. M.; Meerts, W. L. *J. Phys. Chem.* **1990**, *94*, 6−8.
(75) Rice, J. K.; Baronavski, A. P. *J. Phys. Chem.* **1992**, *96*, 3359−3366.
(76) Baranovic, G. *J. Raman. Spectrosc.* **2001**, *32*, 293−299.
(77) Kwok, M. W.; Ma, C.; Phillips, D.; Beeby, A.; Marder, T. B.; Thomas, R. Ll.; Tschuschke, C.; Baranovic, G.; Matousek, P.; Towrie, M.; Parker, A. W. *J. Raman. Spectrosc.* **2003**, *34*, 886−891.
(78) Bao, J.; Weber, P. M. *J. Phys. Chem. Lett.* **2010**, *1*, 224−227.
(79) Bao, J.; Minitti, M. P.; Weber, P. M. *J. Phys. Chem. A* **2011**, *115*, 1508−1515.
(80) Bao, J.; Weber, P. M. *J. Am. Chem. Soc.* **2011**, *133*, 4164−4167.
(81) Briney, K. A.; Herman, L.; Boucher, D. S.; Dunkelberger, A. D.; Crim, F. F. *J. Phys. Chem. A* **2010**, *114*, 9788−9794.
(82) Warshel, A. *J. Chem. Phys.* **1975**, *62*, 214−221.
(83) Orlandi, G.; Siebrand, W. *Chem. Phys. Lett.* **1975**, *30*, 352−354.
(84) Negri, F.; Orlandi, G. *J. Phys. Chem.* **1991**, *95*, 748−757.
(85) Tavan, P.; Schulten, K. *Chem. Phys. Lett.* **1978**, *56*, 200−204.
(86) Troe, J. *Chem. Phys. Lett.* **1985**, *114*, 241−247.
(87) Nordholm, S. *Chem. Phys.* **1989**, *137*, 109−120.
(88) Bolton, K.; Nordholm, S. *Chem. Phys.* **1996**, *203*, 101−126.
(89) Troe, J.; Weitzel, K.-M. *J. Chem. Phys.* **1988**, *88*, 7030−7039.
(90) Schroeder, J.; Steinel, T.; Troe, J. *J. Phys. Chem. A* **2002**, *106*, 5510−5516.
(91) Petek, H.; Fujiwara, Y.; Kim, D.; Yoshihara, K. *J. Am. Chem. Soc.* **1988**, *110*, 6269−6270.
(92) Petek, H.; Yoshihara, K.; Fujiwara, Y.; Lin, Z.; Penn, J. H.; Frederick, J. H. *J. Phys. Chem.* **1990**, *94*, 7539−7543.
(93) Frederick, J. H.; Fujiwara, Y.; Penn, J. H.; Yoshihara, K.; Petek, H. *J. Phys. Chem.* **1991**, *95*, 2845−2858.
(94) Bearpark, M. J.; Bernardi, F.; Clifford, S.; Olivucci, M.; Robb, M. A.; Vreven, T. *J. Phys. Chem. A* **1997**, *101*, 3841−3847.
(95) Molina, V.; Merchán, M.; Roos, B. O. *J. Phys. Chem. A* **1997**, *101*, 3478−3487.
(96) Molina, V.; Merchán, M.; Roos, B. O. *Spectrochim. Acta A* **1999**, *55*, 433−446.
(97) Gagliardi, L.; Orlandi, G.; Molina, V.; Malmqvist, P.-Å.; Roos, B. O. *J. Phys. Chem. A* **2002**, *106*, 7355−7361.
(98) Amatatsu, Y. *Chem. Phys. Lett.* **1999**, *314*, 364−368.
(99) Quenneville, J.; Martínez, T. J. *J. Phys. Chem. A* **2003**, *107*, 829−837.
(100) Leitner, D. M.; Levine, B.; Quenneville, J.; Martínez, T. J.; Wolynes, P. G. *J. Phys. Chem. A* **2003**, *107*, 10706−10716.
(101) Chowdary, P. D.; Martinez, T. J.; Gruebele, M. *Chem. Phys. Lett.* **2007**, *440*, 7−11.
(102) Levine, B. G.; Coe, J. D.; Martínez, T. J. *J. Phys. Chem. B* **2008**, *112*, 405−413.
(103) Kwasniewski, S. P.; Deleuze, M. S.; François, J. P. *Int. J. Quantum Chem.* **2000**, *80*, 672−680.
(104) Claes, L.; Kwasniewski, S.; Deleuze, M. S.; Francois, J.-P. *J. Mol. Struct. (THEOCHEM)* **2001**, *549*, 63−67.
(105) Kwasniewski, S. P.; Claes, L.; François, J.-P.; Deleuze, M. S. *J. Chem. Phys.* **2003**, *118*, 7823−7836.
(106) Improta, R.; Santoro, F.; Dietl, C.; Papastathopoulos, E.; Gerber, G. *Chem. Phys. Lett.* **2004**, *387*, 509−516.
(107) Dietl, C.; Papastathopoulos, E.; Niklaus, P.; Improtra, R.; Santoro, F.; Gerber, G. *Chem. Phys.* **2005**, *310*, 201−211.
(108) Improta, R.; Santoro, F. *J. Phys. Chem. A* **2005**, *109*, 10058−10067.
(109) Angeli, C.; Improta, R.; Santoro, F. *J. Chem. Phys.* **2009**, *130*, 174307.
(110) Gershinsky, G.; Pollak, E. *J. Chem. Phys.* **1997**, *107*, 812−824.
(111) Gershinsky, G.; Pollak, E. *J. Chem. Phys.* **1997**, *107*, 10532−10538.
(112) Tatchen, J.; Pollak, E. *J. Chem. Phys.* **2008**, *128*, 164303.
(113) Vachev, V. D.; Frederick, J. H.; Grishanin, B. A.; Zadkov, V. N.; Koroteev, N. I. *Chem. Phys. Lett.* **1993**, *215*, 306−314.
(114) Vachev, V. D.; Frederick, J. H.; Grishanin, B. A.; Zadkov, V. N.; Koroteev, N. I. *J. Phys. Chem.* **1995**, *99*, 5247−5263.
(115) Berweger, C. D.; van Gunsteren, W. F.; Müller-Plathe, F. *J. Chem. Phys.* **1998**, *108*, 8773−8781.
(116) Berweger, C. D.; van Gunsteren, W. F.; Müller-Plathe, F. *J. Chem. Phys.* **1999**, *111*, 8987−8999.
(117) Han, W. G.; Lovell, T.; Liu, T.; Noodleman, L. *ChemPhysChem* **2002**, *3*, 167−178.
(118) Chen, P. C.; Chieh, Y. C. *J. Mol. Struct. (THEOCHEM)* **2003**, *624*, 191−200.
(119) Vendrame, R.; Coluci, V. R.; Galvao, D. S. *J. Mol. Struct. (THEOCHEM)* **2004**, *686*, 103−108.
(120) Dou, Y.; Allen, R. E. *Chem. Phys. Lett.* **2003**, *378*, 323−329.
(121) Dou, Y.; Allen, R. E. *J. Chem. Phys.* **2003**, *119*, 10658−10666.
(122) Dou, Y.; Allen, R. E. *J. Mod. Opt.* **2004**, *51*, 2485−2491.
(123) Dou, Y.; Wu, W.; Tang, H.; Allen, R. E. *Chem. Phys.* **2008**, *353*, 104−108.
(124) Jiang, C.-W.; Xie, R.-H.; Li, F.-L.; Allen, R. E. *Chem. Phys. Lett.* **2009**, *474*, 263−267.
(125) Jiang, C.-W.; Xie, R.-H.; Li, F.-L.; Allen, R. E. *Chem. Phys. Lett.* **2010**, *487*, 177−182.

(126) Weston, R. E., Jr.; Barker, J. R. *J. Phys. Chem A.* **2006**, *110*, 7888−7897.
(127) Debnarova, A.; Techert, S.; Schmatz, S. *J. Chem. Phys.* **2006**, *125*, 224101.
(128) Tranca, D. C.; Neufeld, A. A. *J. Chem. Phys.* **2010**, *132*, 134109.
(129) Minezawa, N.; Gordon, M. S. *J. Phys. Chem. A* **2011**, *115*, 7901−7911.
(130) Tzeli, D.; Theodorakopoulos, G.; Petsalakis, I. D.; Ajami, D.; Rebek, D., Jr *J. Am. Chem. Soc.* **2012**, *134*, 4346−4354.
(131) Chaudhuri, R. K.; Freed, K. F.; Chattopadhyay, S.; Mahapatra, U. S. *J. Phys. Chem. A* **2013**, *117*, 9424−9434.
(132) Granovsky, A. A. *J. Chem. Phys.* **2011**, *134*, 214113.
(133) Nakano, H. *J. Chem. Phys.* **1993**, *99*, 7983−7992.
(134) Nakano, H. *Chem. Phys. Lett.* **1993**, *207*, 372−378.
(135) Shiozaki, T.; Gyorffy, W.; Celani, P.; Werner, H. J. *J. Chem. Phys.* **2011**, *135*, 081106.
(136) Granovsky, A. A. *Firefly version 8.0.0*. http://classic.chem.msu.su/gran/firefly/index.html (accessed September 15, 2013).
(137) Schmidt, M. W.; Baldridge, K. K.; Boatz, J. A.; Elbert, S. T.; Gordon, M. S.; Jensen, J. H.; Koseki, S.; Matsunaga, N.; Nguyen, K. A.; Su, S.; Windus, T. L.; Dupuis, M.; Montgomery, J. A. *J. Comput. Chem.* **1993**, *14*, 1347−1363.
(138) Bonačič-Koutecký, V.; Bruckmann, P.; Hiberty, P.; Koutecký, J.; Leforestier, C.; Salem, L. *Angew. Chem., Int. Ed.* **1975**, *14*, 575−576.
(139) Bersuker, I. B. *Chem. Rev.* **2013**, *113*, 1351−1390.
(140) Malrieu, P. P.; Heully, J. L.; Zaitsevskii, A. *Theor. Chim. Acta* **1995**, *90*, 167−187.
(141) Zhurko, G. *Chemcraft version 1.7*. www.chemcraftprog.com (accessed September 15, 2013).
(142) Cerbere, G.; De Luca, G.; Di Pieto, M. E. *J. Phys. Chem. B* **2012**, *116*, 2876−2885.
(143) Rademacher, P.; Marzinzik, A. L.; Kowski, K.; Weiss, M. E. *Eur. J. Org. Chem.* **2001**, 121−130.
(144) Traetteberg, M.; Frantsen, E. B.; Mijlhoff, F. C.; Hoekstra, A. *J. Mol. Struct.* **1975**, *26*, 57−68.
(145) Hoekstra, A.; Meertens, P.; Vos, A. *Acta Crystallogr. B* **1975**, *31*, 2813−2817.
(146) Cammenga, H. K.; Emel'yanenko, V. N.; Verevkin, S. P. *Ind. Eng. Chem. Res.* **2009**, *48*, 10120−10128.
(147) Saltiel, J.; Ganapathy, S.; Werking, C. *J. Phys. Chem.* **1987**, *91*, 2755−2758.
(148) Kvaran, A.; Konradsson, A. E.; Evans, C.; Geirsson, J. F. K. *J. Mol. Struct.* **2000**, *553*, 79−90.
(149) Gozem, S.; Huntress, M.; Schapiro, I.; Lindh, R.; Granovsky, A. A.; Angeli, C.; Olivucci, M. *J. Chem. Theory Comput.* **2012**, *8*, 4069−4080.
(150) Celani, P.; Garavelli, M.; Ottani, S.; Bernardi, F.; Robb, M. A.; Olivucci, M. *J. Am. Chem. Soc.* **1995**, *117*, 11584−11585.
(151) Garavelli, M.; Celani, P.; Bernardi, F.; Robb, M. A.; Olivucci, M. *J. Am. Chem. Soc.* **1997**, *119*, 11487−11494.
(152) Sadovnichy, V.; Tikhonravov, A.; Voevodin, Vl.; Opanasenko, V. "Lomonosov": Supercomputing at Moscow State University. In *Contemporary High Performance Computing: From Petascale toward Exascale*; Vetter, J. S., Ed.; Chapman & Hall/CRC Computational Science series; CRC Press: Boca Raton, FL, 2013; pp 283−307.